Numerically explicit potentials for the homogenization of nonlinear elastic heterogeneous materials

Julien Yvonnet, D. Gonzalez, Qi-Chang He

Numerically explicit potentials for the homogenization of nonlinear elastic heterogeneous materials

J. Yvonnet [a,*], D. Gonzalez [b], Q.-C. He [a]

[a] *Université Paris-Est, Laboratoire Modélisation et Simulation Multi Échelle, FRE 3160 CNRS,*
5 Bd Descartes, 77454 Marne-la-Vallée Cedex, France

[b] *Group of Structural Mechanics and Material Modelling. Aragon Institute of Engineering Research (I3A). University of Zaragoza. Mara de Luna, 5. Campus Rio Ebro. E-50018 Zaragoza, Spain.*

Abstract

The homogenization of nonlinear heterogeneous materials is much more difficult than the homogenization of linear ones. This is mainly due to the fact that the general form of the homogenized behavior of nonlinear heterogeneous materials is unknown. At the same time, the prevailing numerical methods, such as concurrent methods, require extensive computational efforts. A simple numerical approach is proposed to compute the effective behavior of nonlinearly elastic heterogeneous materials at small strains. The proposed numerical approach comprises three steps. At the first step, a representative volume element (RVE) for a given nonlinear heterogeneous material is defined, and a loading space consisting of all the boundary conditions to be imposed on the RVE is discretized into a sufficiently large number of points called nodes. At the second step, the boundary condition corresponding to each node is prescribed on the surface of the RVE, and the resulting nonlinear boundary value problem, is solved by the finite element method (FEM) so as to determine the effective response of the heterogeneous material to the loading associated to each node of the loading space. At the third step, the nodal effective responses are interpolated via appropriate interpolation functions, so that the effective strain energy, stress-strain relation and tangent stiffness tensor of the nonlinear heterogeneous material are provided in a numerically explicit way. This leads to a non-concurrent nonlinear multiscale approach to the computation of structures made of nonlinearly heterogeneous materials. The first version of the proposed approach uses mutidimensional cubic splines to interpolate effective nodal responses while the second version of the proposed approach takes advantage of an outer product decomposition of multidimensional data into rank-one tensors to interpolate effective nodal responses and avoid high-rank data. These two versions of the proposed approach are applied to a few examples where nonlinear composites whose

phases are characterized by the power-law model are involved. The numerical results given by our approach are compared with available analytical estimates, exact results and full FEM or concurrent multilevel FEM solutions.

Key words: Nonlinear composites, Separated representation, Numerically explicit potentials, Constitutive models, Multiscale methods

1 Introduction

The homogenization of nonlinear heterogeneous materials is by an order of magnitude tougher than the homogenization of linear ones. The main reason is that: (a) in the linear case, the general form of the homogenized (or effective) behavior of heterogeneous materials is a priori known and it suffices to determine a set of effective moduli by considering a finite number of macroscopic loading modes; (b) in contrast, in the nonlinear case, the general form of the homogenized behavior of heterogeneous materials is unknown and the determination of the homogenized behavior requires solving nonlinear partial differential equations with random or periodic coefficients and entails considering, in principle, an infinite number of macroscopic loading modes. Many analytical and numerical works have been devoted to the homogenization of nonlinear heterogeneous materials

The analytical methods which have been proposed since the pioneer work of Hill [1] aim at estimating or bounding the effective behavior of nonlinear heterogeneous materials. These methods, including the ones proposed by Willis [2], Dvorak [3], Qiu and Weng [4], Ponte Castañeda [5], Hu [6], Milton and Serkov [7], can be viewed as extending to the nonlinear case of some well-established techniques available for estimating or bounding the effective behavior of linear heterogeneous materials (see., e.g., Nemat-Nasser & Hori [8]; Torquato [9]; Milton [10]). At the same time, a few exact results have been obtained for nonlinear heterogeneous materials presenting simple microstructures and undergoing particular loadings [11–15]. The analytical estimates, bounds and exact results reported in the literature on the homogenization of nonlinear heterogeneous materials are of both theoretical and practical importance. However, due to the difficulties inherent in analytically solving nonlinear homogenization problems, all of them have been obtained under rather restrictive assumptions and are not sufficient for the computation of structures

* Correspondence to J. Yvonnet
Email address: julien.yvonnet@univ-paris-est.fr (J. Yvonnet).

consisting of nonlinear heterogeneous materials of complex microstructure and subjected to arbitrary macroscopic loadings.

In spite of the recent drastic increase in the performance of computers, full-field (or direct) numerical simulations of a structure made of a nonlinear medium of high heterogeneity remain expensive and may be beyond available computer capacity. The basic idea underlying the currently prevailing computational methods for dealing with a structure composed of a nonlinear heterogeneous material is to first associate each macroscopic integration point with a representative volume element (RVE) of the material, then prescribe the macroscopic strain relative to the integration point as the boundary conditions for the RVE, and finally solve the relevant homogenization problem for every increment of the macroscopic loading imposed on the structure. These methods, found in the literature under the names such as "Concurrent Multiscale Methods", "Multilevel Finite Element" and "Computational Homogenization" (see, e.g., [16–24]) show many attractive features in comparison with the aforementioned analytical approaches: (i) the local nonlinear constitutive laws of the phases of the heterogeneous material can be of much more general form; (ii) the microstructure of the heterogeneous material can be very complex and evolving; (iii) loading modes can be arbitrary. However, their main shortcoming is that the computational cost is still high even though use is made of techniques like model reduction [22], [23] or parallel computing [17] to reduce it. More recently, McVeigh et al. [25] developed an alternative approach based on Multiresolution continuum theory to take into account non homogeneous deformations at different scales.

In the present work, we propose a numerical approach to the homogenization of nonlinear heterogeneous materials, which is completely different from the ones reported in the literature and particularly suitable for the computation of structures. The basic idea of our approach is quite simple and can be stated as follows. Given a nonlinear heterogeneous material, we first consider an RVE of it and a loading space consisting of all the boundary conditions to be imposed on the RVE. The loading space, or a domain of relevance of the latter, is then discretized with the help of a sufficiently large number of points called nodes. The boundary condition corresponding to each node is prescribed on the surface of the RVE and the resulting nonlinear boundary value problem is solved by the finite element method (FEM). Thus, the effective energy response of the nonlinear heterogeneous material in question is numerically determined for each node of the loading space. Finally, the effective response of the nonlinear heterogeneous material evaluated for any point of the loading space is constructed by interpolating the nodal effective responses via appropriate interpolation functions and their derivatives. The effective behavior of the nonlinear heterogeneous material thus obtained is numerically general and explicit, allowing the replacement of the nonlinear heterogeneous material by the homogenized one in the case of carrying out structural computation. Even

though the basic idea of our approach is applicable to a large class of nonlinear heterogeneous materials based on a smooth convex potential, the present work is limited to nonlinearly elastic heterogeneous materials subjected to small deformations.

The paper is organized as follows. In section 2, we recall the equations governing the homogenization of nonlinearly elastic heterogeneous materials at small strains. Section 3 is dedicated to presenting the numerical approach proposed to determine the effective strain-energy function for deriving the overall stress-strain relation and tangent stiffness tensor. In section 4, the proposed numerical approach is tested and illustrated through several examples where nonlinear composites whose phases are characterized by the power-law model are involved. The numerical results provided by our approach are compared not only with the corresponding full-field simulations to assess its accuracy and efficiency but also with the relevant estimates and exact results to show its consistency. Our approach is also applied to the bending of a beam made of a nonlinearly elastic heterogeneous material. A few concluding remarks are drawn in the last section.

2 Homogenization of nonlinear elastic composites

This work is concerned with estimating the effective or homogenized behavior of nonlinear elastic composites undergoing small deformations. We consider a representative volume element (r.v.e) Ω of such a composite consisting of N homogeneous elastic phases. The subdomain of Ω occupied by phase $r \in \{1, 2, ..., N\}$ is denoted by Ω_r and described by the characteristic function $\chi^{(r)}$ such that $\chi^{(r)}(\mathbf{x}) = 1$ for $\mathbf{x} \in \Omega_r$ and $\chi^{(r)}(\mathbf{x}) = 0$ for $\mathbf{x} \notin \Omega_r$. We shall symbolize the volume average over Ω_r by $\langle . \rangle_r$ and the one over Ω by $\langle . \rangle$. In particular, $c^{(r)} = \left\langle \chi^{(r)} \right\rangle$ is the volume fraction of phase r. The interfaces between the phases of the composite are taken to be perfect.

Let be given the local strain-energy density function w of the composite under investigation by

$$w(\mathbf{x}, \boldsymbol{\varepsilon}) = \sum_{r=1}^{N} \chi^{(r)}(\mathbf{x}) w^{(r)}(\boldsymbol{\varepsilon}), \tag{1}$$

where $w^{(r)}$ is the strain-energy density function of phase r and $\boldsymbol{\varepsilon}$ is the infinitesimal strain tensor related to the displacement vector $\mathbf{u}$ via

$$\boldsymbol{\varepsilon} = \boldsymbol{\varepsilon}(\mathbf{u}) = \frac{1}{2}[\nabla \mathbf{u} + (\nabla \mathbf{u})^T]. \tag{2}$$

In what follows, each strain energy function $w^{(r)}$ is assumed to be convex but not necessarily quadratic with respect to $\boldsymbol{\varepsilon}$. The local stress-strain relation of the composite is then provided by

$$\boldsymbol{\sigma} = \frac{\partial w(\mathbf{x}, \boldsymbol{\varepsilon})}{\partial \boldsymbol{\varepsilon}}, \tag{3}$$

where $\boldsymbol{\sigma}$ is the Cauchy stress tensor which must satisfy the equilibrium equation:

$$\mathbf{div}(\boldsymbol{\sigma}) = \mathbf{0} \tag{4}$$

in the absence of body forces.

As usual in micromechanics, the macroscopic (or overall) strain and stress tensors, $\bar{\boldsymbol{\varepsilon}}$ and $\bar{\boldsymbol{\sigma}}$, are defined as the volume averages of the local counterparts:

$$\bar{\boldsymbol{\varepsilon}} = \langle \boldsymbol{\varepsilon} \rangle \,, \quad \bar{\boldsymbol{\sigma}} = \langle \boldsymbol{\sigma} \rangle \,. \tag{5}$$

In the case of a composite with cracks, voids and rigid inhomogeneities, the foregoing definitions for the macroscopic strain and stress tensors have to be extended. The boundary conditions (b.c.) considered in this work is either of the following three ones:

(a) uniform traction b.c., i.e.,

$$\boldsymbol{\sigma}\mathbf{n} = \bar{\boldsymbol{\sigma}}\mathbf{n} \quad \text{on} \quad \partial\Omega \tag{6}$$

where $\mathbf{n}$ is the outward unit normal to $\partial\Omega$;

(b) uniform strain b.c., i.e.,

$$\mathbf{u} = \bar{\boldsymbol{\varepsilon}}\mathbf{x} \quad \text{on} \quad \partial\Omega; \tag{7}$$

(c) periodical b.c., i.e.,

$$\mathbf{u} - \bar{\boldsymbol{\varepsilon}}\mathbf{x} \text{ is periodical and } \boldsymbol{\sigma}\mathbf{n} \text{ is anti-periodical on } \partial\Omega. \tag{8}$$

In short, equations (1)-(5) with either of the b.c. (6)-(8) formulate the nonlinear elastic boundary value problem for determining the effective stress-strain relation of the composite. This problem can be conveniently formulated in a variational way. For example, when the boundary conditions (7) are prescribed, the effective strain-energy density function $\bar{w}$ of the composite is obtained by solving the following minimization problem:

$$\bar{w}(\bar{\boldsymbol{\varepsilon}}) = \inf_{\mathbf{v} \in \mathcal{K}(\bar{\boldsymbol{\varepsilon}})} \langle w(\mathbf{x}, \boldsymbol{\varepsilon}(\mathbf{v})) \rangle \tag{9}$$

where $\mathcal{K}(\bar{\boldsymbol{\varepsilon}})$ is the space of all displacements $\mathbf{v}$ defined over Ω and verifying the boundary conditions $\mathbf{u} = \bar{\boldsymbol{\varepsilon}}\mathbf{x}$ on $\partial\Omega$. It can be shown that $\bar{w}$ is a convex function of $\bar{\boldsymbol{\varepsilon}}$ provided w is convex with respect to $\boldsymbol{\varepsilon}$ ([26]). Further, the effective stress-strain relation is given by (see, e.g., [27])

$$\bar{\boldsymbol{\sigma}} = \frac{\partial \bar{w}(\bar{\boldsymbol{\varepsilon}})}{\partial \bar{\boldsymbol{\varepsilon}}}. \tag{10}$$

The main purpose of what follows is to provide a twice continuously differentiable numerical estimation for the effective strain-energy density function $\bar{w}$.

3 Construction of numerically explicit potentials for the homogenized behavior of nonlinear elastic composites

When a linearly elastic composite is concerned, the effective strain-energy density $\bar{w}$, referred to simply as potential, is a quadratic function defined over the space $\mathcal{E}$ of macroscopic infinitesimal strain tensors $\bar{\boldsymbol{\varepsilon}}$, which is in the most general case characterized by 21 effective elastic moduli. In this sense, $\bar{w}$ is said to have an exact discrete representation. When a nonlinearly elastic composite is under investigation, the form of $\bar{w}$ as a function defined over $\mathcal{E}$ is in general unknown and cannot be exactly specified in terms of a finite number of parameters. In other words, $\bar{w}$ has not an exact finite representation. However, once $\bar{w}$ has been accurately evaluated for a sufficient number of points of $\mathcal{E}$, we expect that, under certain regularity conditions for $\bar{w}$, there is a good continuous but finite approximation $\bar{w}^*$ for $\bar{w}$ such that $\bar{w}^*(\bar{\boldsymbol{\varepsilon}})$ is close enough to $\bar{w}(\bar{\boldsymbol{\varepsilon}})$ for any point $\bar{\boldsymbol{\varepsilon}}$ of $\mathcal{E}$.

In this work, we first consider an RVE Ω of the nonlinearly elastic composite and accurately estimate $\bar{w}$ for a sufficient number of points of $\mathcal{E}$ by the finite element method. Then, a "Numerically Explicit Potential" (NEXP for short), i.e. a continuous finite approximation $\bar{w}^*$ of $\bar{w}$, is constructed by interpolating the computed discrete values of $\bar{w}$. The interpolation functions used are required to be twice continuously differentiable (or $\mathcal{C}^2$), so that we can finally obtain the approximated effective stress-strain relation and tangent stiffness tensor by calculating the first and second derivatives of $\bar{w}^*$.

3.1 Notational preliminaries

The space $\mathcal{E}$ consisting of all macroscopic strain tensors $\bar{\boldsymbol{\varepsilon}}$ will be referred to as the loading space, since, in the following, the macroscopic variable prescribed

on the boundary $\partial\Omega$ of Ω is an element $\bar{\boldsymbol{\varepsilon}}$ of $\mathcal{E}$. Let $\{\mathbf{e}_1, \mathbf{e}_2, \mathbf{e}_3\}$ be a three-dimension (3D) orthonormal basis. Usually, $\bar{\boldsymbol{\varepsilon}}$ is decomposed as follows

$$\bar{\boldsymbol{\varepsilon}} = \bar{\varepsilon}_{11}\mathbf{e}_1 \otimes \mathbf{e}_1 + \bar{\varepsilon}_{22}\mathbf{e}_2 \otimes \mathbf{e}_2 + \bar{\varepsilon}_{33}\mathbf{e}_3 \otimes \mathbf{e}_3 + \bar{\varepsilon}_{23}(\mathbf{e}_2 \otimes \mathbf{e}_3 + \mathbf{e}_3 \otimes \mathbf{e}_2)$$

$$+\bar{\varepsilon}_{31}(\mathbf{e}_1 \otimes \mathbf{e}_3 + \mathbf{e}_3 \otimes \mathbf{e}_1) + \bar{\varepsilon}_{12}(\mathbf{e}_1 \otimes \mathbf{e}_2 + \mathbf{e}_2 \otimes \mathbf{e}_1). \tag{11}$$

For our purpose, it is more convenient to use another decomposition of $\bar{\boldsymbol{\varepsilon}}$:

$$\bar{\boldsymbol{\varepsilon}} = \bar{\varepsilon}_1\mathbf{e}_1 \otimes \mathbf{e}_1 + \bar{\varepsilon}_2\mathbf{e}_2 \otimes \mathbf{e}_2 + \bar{\varepsilon}_3\mathbf{e}_3 \otimes \mathbf{e}_3 + \frac{\bar{\varepsilon}_4}{\sqrt{2}}(\mathbf{e}_2 \otimes \mathbf{e}_3 + \mathbf{e}_3 \otimes \mathbf{e}_2)$$

$$+\frac{\bar{\varepsilon}_5}{\sqrt{2}}(\mathbf{e}_1 \otimes \mathbf{e}_3 + \mathbf{e}_3 \otimes \mathbf{e}_1) + \frac{\bar{\varepsilon}_6}{\sqrt{2}}(\mathbf{e}_1 \otimes \mathbf{e}_2 + \mathbf{e}_2 \otimes \mathbf{e}_1)\ . \tag{12}$$

Comparing (11) with (12) gives rise to the relations:

$$\bar{\varepsilon}_1 = \bar{\varepsilon}_{11},\ \bar{\varepsilon}_2 = \bar{\varepsilon}_{22},\ \bar{\varepsilon}_3 = \bar{\varepsilon}_{33},\ \bar{\varepsilon}_4 = \sqrt{2}\bar{\varepsilon}_{23},\ \bar{\varepsilon}_5 = \sqrt{2}\bar{\varepsilon}_{31},\ \bar{\varepsilon}_6 = \sqrt{2}\bar{\varepsilon}_{12}. \tag{13}$$

It is well-known that this notation is mathematically more consistent than the traditional Voigt one. In a similar way, we can introduce the components $\bar{\sigma}_\alpha$ $(\alpha = 1, 2, ..., 6)$ and $\bar{\sigma}_{ij}(i, j = 1, 2, 3)$ of the macroscopic stress tensor $\bar{\sigma}$, which are related by the relations similar to (13).

In the general situation, the potential $\bar{w}$ is defined over $\mathcal{E}$ which can be viewed as a six-dimension vector space, i.e.

$$\bar{w} = \bar{w}(\bar{\varepsilon}_1, \bar{\varepsilon}_2, ..., \bar{\varepsilon}_6), \tag{14}$$

and the effective stress-strain relation and the effective tangent stiffness matrix $\bar{\mathbb{L}} = \partial^2\bar{w}/\partial\bar{\boldsymbol{\varepsilon}}\partial\bar{\boldsymbol{\varepsilon}}$ are given by

$$\bar{\sigma}_\alpha = \frac{\partial\bar{w}}{\partial\bar{\varepsilon}_\alpha}, \quad \bar{L}_{\alpha\beta} = \gamma\hat{L}_{\alpha\beta}\ \ , \hat{L}_{\alpha\beta} = \frac{\partial^2\bar{w}}{\partial\bar{\varepsilon}_\alpha\partial\bar{\varepsilon}_\beta}. \tag{15}$$

where the values of γ for the different combinations of α and β are provided in Appendix 2. However, we are sometimes interested only in a particular problem, for example a plane-strain problem relative to the plane $x_1 - x_2$. In such a case, $\bar{w}$ depends only on $\bar{\varepsilon}_1$, $\bar{\varepsilon}_2$ and $\bar{\varepsilon}_6$, and the value range of the suffixes α and β in (15) are $\{1, 2, 6\}$. In this section, we focus our attention only on the general situation. When a specific problem is in question, it is relatively easy to adapt the general method presented in this section.

3.1.1 Discrete representation of the potential

First, we carry out the discretization of the six-dimension loading space $\mathcal{E}$. A general non-uniform discretization can be envisaged. However, for the sake of simplicity, we only present the case of regular discretization in the following. For this, the $\bar{\varepsilon}_\alpha$-axe associated with the effective strain component $\bar{\varepsilon}_\alpha$ with $\alpha = 1, 2, ..., 6$ is uniformly graduated. Note that $\bar{\varepsilon}_\alpha$ has to vary between a certain minimum value $\bar{\varepsilon}_\alpha^{\min}$ and a certain maximum value $\bar{\varepsilon}_\alpha^{\max}$ imposed by the hypothesis of small strains made in this work. A uniform graduation of any $\bar{\varepsilon}_\alpha$-axe limited to the interval $[\bar{\varepsilon}_\alpha^{\min}, \bar{\varepsilon}_\alpha^{\max}]$ can be obtained by introducing a set of points $\{\xi_0^\alpha, \xi_1^\alpha, ..., \xi_{m_\alpha}^\alpha\}$ such that $\bar{\varepsilon}_\alpha^{\min} = \xi_0^\alpha < \xi_1^\alpha < ... < \xi_{m_\alpha}^\alpha = \bar{\varepsilon}_\alpha^{\max}$ and $\xi_1^\alpha - \xi_0^\alpha = \xi_2^\alpha - \xi_1^\alpha = ... = \xi_{m_\alpha}^\alpha - \xi_{m_\alpha - 1}^\alpha$. Thus, the subdomain $\Delta = [\bar{\varepsilon}_1^{\min}, \bar{\varepsilon}_1^{\max}] \times [\bar{\varepsilon}_2^{\min}, \bar{\varepsilon}_2^{\max}] \times ... \times [\bar{\varepsilon}_6^{\min}, \bar{\varepsilon}_6^{\max}]$ of $\mathcal{E}$ is discretized into a uniform grid. A node of Δ is a point $(\xi_{i_1}^1, \xi_{i_2}^2, ..., \xi_{i_6}^6)$ with $0 \leq i_\alpha \leq m_\alpha$. In this work, we set $m_1 + 1 = m_2 + 1 = ... = m_6 + 1 = p$ so that Δ contains p^6 nodes.

Next, we evaluate $\bar{w}$ at each node of Δ by FEM. More Precisely, given the effective strain components $(\xi_{i_1}^1, \xi_{i_2}^2, ..., \xi_{i_6}^6)$ corresponding to the node $i_1 i_2 ... i_6$ with $0 \leq i_\alpha \leq p - 1$, we apply FEM to solve the nonlinearly elastic boundary value problem for an RVE Ω of the composite, which has been formulated in the foregoing section. Let $\mathbf{u}(\mathbf{x}; \xi_{i_1}^1, \xi_{i_2}^2, ..., \xi_{i_6}^6)$ be the corresponding displacement field obtained by FEM. Then, the evaluation of $\bar{w}$ at the node $i_1 i_2 ... i_6$ is given by

$$\bar{w}(\xi_{i_1}^1, \xi_{i_2}^2, ..., \xi_{i_6}^6) =< w[\mathbf{x}, \varepsilon(\mathbf{u}(\mathbf{x}; \xi_{i_1}^1, \xi_{i_2}^2, ..., \xi_{i_6}^6))] > . \tag{16}$$

For later use, the value of $\bar{w}$ evaluated at the node $i_1 i_2 ... i_6$ is designated by $\bar{w}_{i_1 i_2 ... i_6}$, via

$$\bar{w}_{i_1 i_2 ... i_6} = \bar{w}(\xi_{i_1}^1, \xi_{i_2}^2, ..., \xi_{i_6}^6). \tag{17}$$

Further, we introduce a "hypermatrix" $\bar{\mathbb{W}}$ whose components are constituted of all the elements $\bar{w}_{i_1 i_2 ... i_6}$ $(1 \leq i_\alpha \leq m_\alpha)$, symbolically writing

$$\bar{\mathbb{W}} = [\bar{w}_{i_1 i_2 ... i_6}] \ . \tag{18}$$

In figure 1, an illustration of the discretized strain domain Δ for a problem involving the three macroscopic strain components $\bar{\varepsilon}_1 = \bar{\varepsilon}_{11}$, $\bar{\varepsilon}_2 = \bar{\varepsilon}_{22}$, $\bar{\varepsilon}_6 = \sqrt{2}\bar{\varepsilon}_{12}$ is provided. Some finite element solutions corresponding to the associated deformation states are shown for illustration.

In sum, after solving p^6 boundary value problems by FEM, we have the estimations $\bar{w}_{i_1 i_2 ... i_6}$ of $\bar{w}$ for p^6 nodes. These estimations constitute the discrete representation of $\bar{w}$. By properly interpolating the nodal data $\bar{w}_{i_1 i_2 ... i_6}$ with $0 \leq i_\alpha \leq p - 1$, we can obtain a continuous finite approximation $\bar{w}^*$ of $\bar{w}$. Note that for a problem involving less macroscopic strain components (e.g.

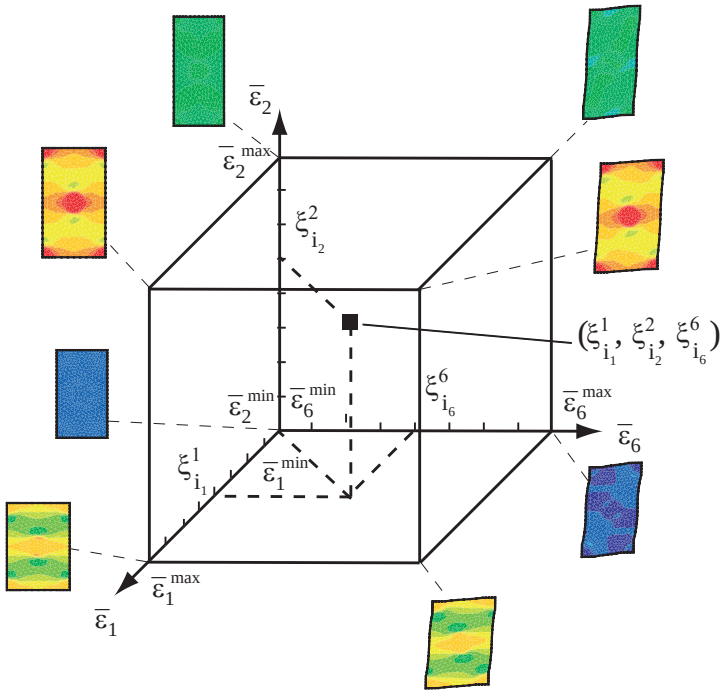

Fig. 1. Discretized strain domain Δ for a problem involving three independent macroscopic strain components. The deformation states associated to some finite element solutions are shown for illustration.

2D problems), we only have to solve p^d boundary value problems for p^d nodes, d being the number of macroscopic strain components. In the following, we describe two techniques for carrying out the interpolation. The first resorts to a multidimensional spline interpolation method. The second technique takes advantage of an outer product decomposition of the data $\bar{w}_{i_1 i_2 \dots i_6}$ and requires only the storage of one-dimensional data among $\bar{w}_{i_1 i_2 \dots i_6}$.

3.2 Direct multidimensional interpolation approach

In this paragraph, we describe a direct interpolation approach (referred to as NEXP1) of the data $\bar{w}_{i_1 i_2 \dots i_6}$ using a multidimensional spline interpolation technique. To satisfy the requirement that a continuous finite approximation $\bar{w}^*$ of $\bar{w}$ be $\mathcal{C}^2$, we choose cubic spline functions. For the sake of the reader, the one-dimensional cubic spline interpolation for regularly distributed nodes is reviewed in Appendix 1. In the following, we apply the multidimensional spline interpolation procedure as detailed in [28].

Given the aforementioned discretization of the domain Δ of $\mathcal{E}$ and the nodal estimations $\bar{w}_{i_1 i_2 \dots i_6}$ of $\bar{w}$, we are looking for a continuous approximation $\bar{w}^*$

of $\bar{w}$ such that

$$\bar{w}^*(\xi^1_{i_1}, \xi^2_{i_2}, ..., \xi^6_{i_6}) = \bar{w}_{i_1 i_2 ... i_6}, \quad 0 \leq i_\alpha \leq p-1. \tag{19}$$

This is accomplished by interpolating the nodal estimations $\bar{w}_{i_1 i_2 ... i_6}$ with the help of the cubic spline functions:

$$\bar{w}^*(\bar{\varepsilon}_1, \bar{\varepsilon}_2, ..., \bar{\varepsilon}_6) = \sum_{i_1=1}^{p+2} ... \sum_{i_6=1}^{p+2} c_{i_1 i_2 ... i_6} \prod_{j=1}^{6} \phi^j_{i_j}(\bar{\varepsilon}_j). \tag{20}$$

In this expression, the cubic spline functions $\phi^j_{i_j}$ are defined by

$$\phi^j_{i_j}(\bar{\varepsilon}_j) = \Phi\left(\frac{\bar{\varepsilon}_j - \bar{\varepsilon}^{\min}_j}{h_j} + 2 - i_j\right) \tag{21}$$

where $h_j = (\bar{\varepsilon}^{\min}_j - \bar{\varepsilon}^{\max}_j)/m_j$ and

$$\Phi(t) = \begin{cases} (2-|t|)^3, & 1 \leq |t| \leq 2; \\ 4 - 6\,|t|^2 + 3\,|t|^3\,, & |t| \leq 1; \\ 0, & \text{elsewhere.} \end{cases} \tag{22}$$

The coefficients $c_{i_1 i_2 ... i_6}$ are obtained by exploiting the interpolation conditions (19). The size of this problem is $\prod_{j=1}^{d}(m_j + 3)$. An efficient algorithm to determine the coefficients $c_{i_1 i_2 ... i_6}$ is provided in [28]. Efficient routines for multidimensional splines are readily available, e.g. in the Matlab® code ("interpn.m" function with "spline" argument).

We can then express the stress-strain relationship in a numerically explicit way:

$$\bar{\sigma}^*_k(\bar{\varepsilon}_1, \bar{\varepsilon}_2, ..., \bar{\varepsilon}_6) = \frac{\partial \bar{w}^*(\bar{\varepsilon}_1, \bar{\varepsilon}_2, ..., \bar{\varepsilon}_6)}{\partial \bar{\varepsilon}_k} =$$

$$= \sum_{i_1=1}^{p+2} ... \sum_{i_6=1}^{p+2} c_{i_1 i_2 ... i_6} \left\{ \prod_{j \neq k}^{6} \phi^j_{i_j}(\bar{\varepsilon}_j) \right\} \frac{\partial \phi^k_{i_k}(\bar{\varepsilon}_k)}{\partial \bar{\varepsilon}_k}\ . \tag{23}$$

The effective elastic tangent moduli can then be calculated by Eq. (15) with

$$\hat{L}^*_{kl}(\bar{\varepsilon}_1, \bar{\varepsilon}_2, ..., \bar{\varepsilon}_6) = \frac{\partial^2 \bar{w}^*(\bar{\varepsilon}_1, \bar{\varepsilon}_2, ..., \bar{\varepsilon}_6)}{\partial \bar{\varepsilon}_k \partial \bar{\varepsilon}_l}$$

$$= \sum_{i_1=1}^{p+2} ... \sum_{i_6=1}^{p+2} c_{i_1 i_2 ... i_6} \left\{ \prod_{j \neq k,l}^{6} \phi_{i_j}^{j}(\bar{\varepsilon}_j) \right\} \frac{\partial \phi_{i_k}^{k}(\bar{\varepsilon}_k)}{\partial \bar{\varepsilon}_k} \frac{\partial \phi_{i_l}^{l}(\bar{\varepsilon}_l)}{\partial \bar{\varepsilon}_l} \text{ if } k \neq l \tag{24}$$

$$\hat{L}_{kl}^{*}(\bar{\varepsilon}_1, \bar{\varepsilon}_2, ..., \bar{\varepsilon}_6) =$$

$$= \sum_{i_1=1}^{p+2} ... \sum_{i_6=1}^{p+2} c_{i_1 i_2 ... i_6} \left\{ \prod_{j \neq l}^{6} \phi_{i_j}^{j}(\bar{\varepsilon}_j) \right\} \frac{\partial^2 \phi_{i_l}^{l}(\bar{\varepsilon}_l)}{\partial \bar{\varepsilon}_l^2} \text{ if } k = l. \tag{25}$$

The convergence of such an interpolation scheme with respect to the number of points p is ensured by the classical polynomial approximation theory, and is discussed in [29]. For 2D problems involving 2 or 3 strains components, this first technique runs very fast, even for relatively fine grids. However, for 3D problems involving 6 strain components, finding the coefficients $c_{i_1 i_2 ... i_6}$ implies solving a very large system of equations, and requires extensive computational time and memory. In the next section, an alternative technique is proposed which avoids these drawbacks.

3.3 Separated variables interpolation approach

The outer product decomposition of a multidimensional data grid into rank-one tensors goes back to Hitchkock [30]. It was later rediscovered independently and called differently such as Parallel Factors [31], Canonical Decomposition [32], Topographic Component Model [33] or parallel factors (PARAFAC) decomposition [34]. The PARAFAC decomposition factorizes a tensor into a sum of rank-one tensors. Another tensor decomposition closely related is the Higher-Order Singular Value Decomposition (HOSVD) [35], also called N-mode principal components analysis [36], or three mode factor analysis (3MFA/Tucker3) [37]. As compared to the PARAFAC decomposition, the HOSVD introduces a core tensor in the tensor outer product (see [37]). Muti and Bourennane [38] used the HOSVD for multidimensional signal analysis. Beylkin and Molhenkamp [39] elaborated algorithms based on the separated variable representation to solve high-dimensional linear systems and addressed the issue of conditioning. They also developed techniques for dealing with antisymmetric functions, as arising in the multiparticle Schrödinger equation in quantum mechanics.

In this second approach (referred to as NEXP2), the hypermatrix $\bar{\mathbb{W}}$ defined by (18) is approximated by its separated representation $\bar{\mathbb{U}}$:

$$\bar{\mathbb{W}} \approx \bar{\mathbb{U}}(\xi_{i_1}^1, \xi_{i_2}^2, ..., \xi_{i_6}^6) = \sum_{r=1}^{R} \boldsymbol{\phi}_1^r \otimes \boldsymbol{\phi}_2^r \otimes ... \otimes \boldsymbol{\phi}_6^r \ , \tag{26}$$

where $\boldsymbol{\phi}_i^r$ $(i = 1, ..., 6)$ is the real-valued vector associated with the macroscopic strain tensor component $\bar{\varepsilon}_i$ and R is an integer. In index notation Eq. (26) reads:

$$\bar{w}_{i_1 i_2 ... i_6} \approx \bar{U}_{i_1 i_2 ... i_6} = \sum_{r=1}^{R} \{\phi_1^r\}_{i_1} \{\phi_2^r\}_{i_2} ... \{\phi_6^r\}_{i_6} \ , \tag{27}$$

where $\left\{\phi_j^r\right\}_k$ denotes the k-th entry of vector $\boldsymbol{\phi}_j^r$. The vectors $\boldsymbol{\phi}_j^r$ involved in (26) are found by solving the following least squares problem for a given R:

$$\underset{\boldsymbol{\phi}_j^r}{inf} \quad \left\| \bar{\mathbb{W}} - \sum_{r=1}^{R} \boldsymbol{\phi}_1^r \otimes \boldsymbol{\phi}_2^r \otimes ... \otimes \boldsymbol{\phi}_6^r \right\|^2 \ , \ r = 1, ..., R, \quad j = 1, ..., 6 \ , \tag{28}$$

where $\|.\|$ is the Frobenius norm. To achieve a desired accuracy, R can be increased until:

$$\left\| \bar{\mathbb{W}} - \sum_{r=1}^{R} \boldsymbol{\phi}_1^r \otimes \boldsymbol{\phi}_2^r \otimes ... \otimes \boldsymbol{\phi}_6^r \right\| < \delta \ , \tag{29}$$

where δ is a tolerance parameter. As the problem (28) is nonlinear with respect to the unknown vectors $\boldsymbol{\phi}_j^r$, an iterative procedure is required to solve it. An efficient algorithm is the alternated least squares algorithm [32], [31], [40]. The decomposition (26) is well-known to the community of psychometrics, and efficient routines and software have been developed. In this work, use is made of the "parafac.m" Matlab® routine, which can be downloaded freely from the Matlab Tensor Toolbox package (see [41]).

Once $\bar{\mathbb{U}}$ is computed, an arbitrary value of $\bar{w}$ can be approximated by interpolating the one-dimensional discrete functions $\boldsymbol{\phi}_j^r$. Thus, we obtain a separated variables representation of $\bar{w}^*$ in the form:

$$\bar{w}(\bar{\varepsilon}_1, \bar{\varepsilon}_2, ..., \bar{\varepsilon}_6) \approx \bar{w}^*(\bar{\varepsilon}_1, \bar{\varepsilon}_2, ..., \bar{\varepsilon}_6) = \sum_{r=1}^{R} \tilde{\phi}_1^r(\bar{\varepsilon}_1) \tilde{\phi}_2^r(\bar{\varepsilon}_2) ... \tilde{\phi}_6^r(\bar{\varepsilon}_6) \ , \tag{30}$$

where $\tilde{\phi}_j^r(\bar{\varepsilon}_j)$ are the interpolated values of $\boldsymbol{\phi}_j^r$:

$$\tilde{\phi}_j^r(\bar{\varepsilon}_j) = \sum_{k=1}^{n} N_k(\bar{\varepsilon}_j) \left\{\phi_j^r\right\}_k \ . \tag{31}$$

In Eq. (31), N_k is one-dimensional $\mathcal{C}^2$ interpolation function associated with node k, and n denotes the number of nodes supporting the shape functions $N_k(\bar{\varepsilon}_j)$ whose value at $\bar{\varepsilon}_j$ is different from zero. As previously, the stress can

be expressed by

$$\bar{\sigma}_i^*(\bar{\varepsilon}_1, \bar{\varepsilon}_2, ..., \bar{\varepsilon}_6) = \sum_{r=1}^{R} \left(\left\{ \prod_{k \neq i} \tilde{\phi}_k^r(\bar{\varepsilon}_k) \right\} \frac{\partial \tilde{\phi}_i^r(\bar{\varepsilon}_i)}{\partial \bar{\varepsilon}_i} \right) \ , \tag{32}$$

where

$$\frac{\partial \tilde{\phi}_i^r(\bar{\varepsilon}_i)}{\partial \bar{\varepsilon}_i} = \sum_{k=1}^{n} \frac{\partial N_k(\bar{\epsilon}_i)}{\partial \bar{\epsilon}_i} \left\{ \phi_i^r \right\}_k \ . \tag{33}$$

Then, the approximated value $\hat{\mathbb{L}}^*$ of $\hat{\mathbb{L}}$ is evaluated by:

$$\hat{L}_{ij}^*(\bar{\varepsilon}_1, \bar{\varepsilon}_2, ..., \bar{\varepsilon}_6) = \sum_{r=1}^{R} \left(\left\{ \prod_{k \neq i,j} \tilde{\phi}_k^r(\bar{\varepsilon}_k) \right\} \frac{\partial \tilde{\phi}_i^r(\bar{\varepsilon}_i)}{\partial \bar{\varepsilon}_i} \frac{\partial \tilde{\phi}_j^r(\bar{\varepsilon}_j)}{\partial \bar{\varepsilon}_j} \right) \quad \text{if} \quad i \neq j \ , \tag{34}$$

$$\hat{L}_{ij}^*(\bar{\varepsilon}_1, \bar{\varepsilon}_2, ..., \bar{\varepsilon}_6) = \sum_{r=1}^{R} \left(\left\{ \prod_{k \neq i} \tilde{\phi}_k^r(\bar{\varepsilon}_k) \right\} \frac{\partial^2 \tilde{\phi}_i^r(\bar{\varepsilon}_i)}{\partial \bar{\varepsilon}_i^2} \right) \quad \text{if} \quad i = j \ , \tag{35}$$

with

$$\frac{\partial^2 \tilde{\phi}_i^r(\bar{\varepsilon}_i)}{\partial \bar{\varepsilon}_i^2} = \sum_{k=1}^{n} \frac{\partial^2 N_k(\bar{\epsilon}_i)}{\partial \bar{\epsilon}_i^2} \left\{ \phi_i^r \right\}_k \ . \tag{36}$$

In this work, the functions N_i are chosen to be one-dimensional C^2 cubic spline functions, even though other C^2 interpolation schemes can be considered. For a strain domain of high dimension, this approach only requires finding the coefficients of one-dimensional spline functions, and thus only a small system of equations has to be solved, which saves computational time and memory. Furthermore, the separated representation technique needs only storing one-dimensional discrete functions and thus $p \times d \times R$ values.

3.4 Summary and remarks

Below we sum up the main steps of the proposed approach:

(i) (Preliminary computations) Construct the hypermatrix $\bar{\mathbb{W}}$ by solving p^d finite element problems, d being the dimension of the macroscopic loading space, and p being the number of points along each dimension. In the case of the NEXP2 method, decompose $\bar{\mathbb{W}}$ into rank-one tensors.

(ii) (During the structure problem computation) Compute the effective stress and elastic tangent tensor at each integration point of the macroscopic mesh by interpolation of the effective nodal responses in the strain domain.

At this stage, the following remarks are in order.

(a) The approach provides numerically explicit effective stress-strain relations needed for structural computations in a finite element code. This technique only requires storing a hypermatrix in the case of the NEXP1 version, and discrete 1D functions in the NEXP2 version. The numerical treatment necessary to determining the effective stress and elastic tangent tensors is far less than performing a local nonlinear FE computation as in concurrent methods.

(b) The step (i) can be costly for 3D problems or very complex microstructures. However, as the FE problems for nodal effective responses are independent, parallel computations can be straightforwardly implemented.

(c) As compared with concurrent methods, the present procedure does not entail exchange of information between a macroscopic FE problem and a microscopic FE problem. Once the Numerically Explicit Potential is constructed after the preliminary stages, the stress and elastic tangent tensors can be readily evaluated without any new local FE computations. Nevertheless, the present method is in this work restricted to non-dissipative materials, while concurrent methods have not this limitation.

(d) In concurrent methods, the only way to compute the tangent tensor is to achieve numerical evaluation by a perturbation method [17], implying additional costly finite element computations. In the present method the tangent elastic tensor can be derived explicitly from the NEXP.

(e) In the present framework, the NEXP can be used to solve all the problems with structures made of the same heterogeneous material with different mesh sizes and geometries without additional local nonlinear problem to be solved. Problems in which a nonlinear material exhibits more than 2 length scales can be dealt with.

(f) Any numerical technique can be used to compute the effective potential via a r.v.e: Finite Element Method (FEM), Fast Fourier Transform (FFT)-based approach [42], Extended finite element (see e.g. [43]), etc.

(g) When the phases are described by stress-dependent potentials, our method is still valid provided these potentials are convex. This is because, in this case, we can deduce the strain-dependent potentials from the stress-dependent ones with the help of the Legendre transformation:

$$w(\boldsymbol{\varepsilon}) + w^*(\boldsymbol{\sigma}) = \boldsymbol{\varepsilon} : \boldsymbol{\sigma} \tag{37}$$

(h) In the case of materials with periodical microstructure, the choice of the RVE is in general not unique but the computed strain energy density is not influenced by this choice. However, microstractural randomness and the size of the RVE may strongly influence the computed energy density when the heterogeneous materials in question are non-periodical. In this case, care must be taken to ensure that the effective strain energy density is independent of the RVE modelling to within an fixed error.

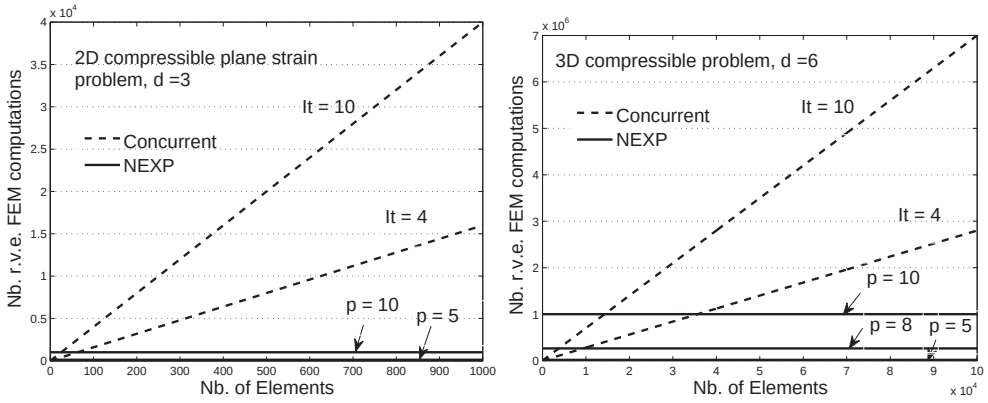

Fig. 2. Nb. of r.v.e. FE computations needed to solve a structure problem with respect to the number of macroscopic structure mesh elements: comparison between concurrent multilevel method and NEXP approaches; (a) 2D compressible plane-strain problem; (b) 3D compressible problem. We set d as the number of independent macroscopic strain components.

3.5 Efficiency analysis

In this section we discuss the advantages of the NEXP method as compared to the concurrent multilevel Finite Element Method in terms of nonlinear FE computations, for solving nonlinear structure problems. In the NEXP method, the total number of FE problems carried out on a r.v.e. is $M = p^d$, where d is the number of independent strain components. In concurrent methods, the total number of FE problems to be solved in a nonlinear structure problem is given by:

$$M = It.Pint.Ne.(1 + Z) \tag{38}$$

where It is the number of iterations until macroscopic equilibrium convergence, $Pint$ is the number of integration points in each element, Ne is the total number of elements in the structure, and $Z = 3$ for 2D problems, and $Z = 6$ for 3D problems. The last term comes from the evaluation of the effective tangent elastic tensor $\bar{\mathbb{L}}$. In the context of concurrent methods, it is required to evaluate $\bar{\mathbb{L}}$ by numerical perturbation, e.g finite differences, which implies $Z = 3$ and $Z = 6$ additional FE computations at each integration point. On the other hand, in the NEXP method context the total number of FE computations only depends on the number p of sampling points along each axis of the multidimensional grid data. In figures 2, we provide a comparison of the numbers of FE computations required in concurrent methods and NEXP methods, respectively, for different cases. It is found that in 2D plane strain problems, the NEXP is much more advantageous, even for coarse macroscopic meshes. For 3D problems, NEXP is also advantageous, as the number of element meshes in that case is usually high.

4 Examples

4.1 Preliminary numerical tests

To test the accuracy and convergence of both NEXP1 and NEXP2 techniques, we first consider an isotropic compressible potential of the form

$$w^{(r)}(\boldsymbol{\varepsilon}) = \frac{9}{2}\kappa^{(r)}\varepsilon_m^2 + \frac{\varepsilon_0^{(r)}\sigma_0^{(r)}}{1+m^{(r)}}\left(\frac{\varepsilon_{eq}}{\varepsilon_0^{(r)}}\right)^{1+m^{(r)}} . \tag{39}$$

In this equation, $\kappa^{(r)}$ denotes the bulk modulus of phase r; $\varepsilon_m = Tr(\boldsymbol{\varepsilon})/3$ is the hydrostatic strain; ε_{eq} is the equivalent strain defined by $\varepsilon_{eq} = \sqrt{2\boldsymbol{\varepsilon}_d : \boldsymbol{\varepsilon}_d/3}$ with $\boldsymbol{\varepsilon}_d = \boldsymbol{\varepsilon} - \varepsilon_m\mathbf{1}$ and $\mathbf{1}$ being the second-order identity tensor. In Eq. (39) $m^{(r)}$ is the strain-hardening parameter of phase r such that $0 \leq m \leq 1$; $\sigma_0^{(r)}$ and $\varepsilon_0^{(r)}$ are the flow stress and reference strain of phase r, respectively. This constitutive model is commonly used to represent a number of nonlinear mechanical phenomena. In particular, the cases $m^{(r)} = 0$ and $m^{(r)} = 1$ are relative to perfectly rigid plastic and linearly elastic materials.

The following numerical parameters are chosen: $\sigma_0^{(r)} = 1$ MPa, $\epsilon_0^{(r)} = 1$, $m^{(r)} = 0.2$, $\kappa^{(r)} = 20$ MPa. Plane strains in the plane $x_1 - x_2$ are assumed. In this case, in order to test the accuracy of both NEXP1 and NEXP2 methods, consider the strain domain $\Delta = [\bar{\varepsilon}_1^{\min}, \bar{\varepsilon}_1^{\max}] \times [\bar{\varepsilon}_2^{\min}, \bar{\varepsilon}_2^{\max}] \times [\bar{\varepsilon}_6^{\min}, \bar{\varepsilon}_6^{\max}] = [-10^{-3}, 10^{-3}] \times [-10^{-3}, 10^{-3}] \times [-10^{-3}, 10^{-3}]$. In figure 3 we plot the potential along the strain path defined by $\bar{\epsilon}_{11} = \bar{\epsilon}_{12}$ and $\bar{\epsilon}_{22} = 0$. For this first test, $p = 21$ points regularly distributed along each dimension of the strain space have been used. The NEXP2 solution is obtained by choosing an accuracy $\delta = 10^{-6}$ leading to $R = 85$. In that case, both method are in very good agreement with the exact solution.

In figure 4, we plot the stress-strain relation computed with the help of NEXP1 and NEXP2. Both of the methods produce oscillations in the vicinity of the zero strain where the slope of the stress-strain relation changes quickly for small values of $m^{(r)}$. This can be expected, as the spline functions cannot reproduce sharp variations. Even though there is room for improvement of the technique, good agreement is noticed with the exact solution, and accuracy is comparable for the two methods.

In figure 5, we depict the tangent stiffness moduli computed by using both NEXP1 and NEXP2. Oscillations are here again noticed, as the values represent derivatives of the stress-strain relation. However, the solutions exhibit reasonable accuracy in the neighborhood of the zero strain state, and are in good agreement with the exact values when strain is quite different from zero.

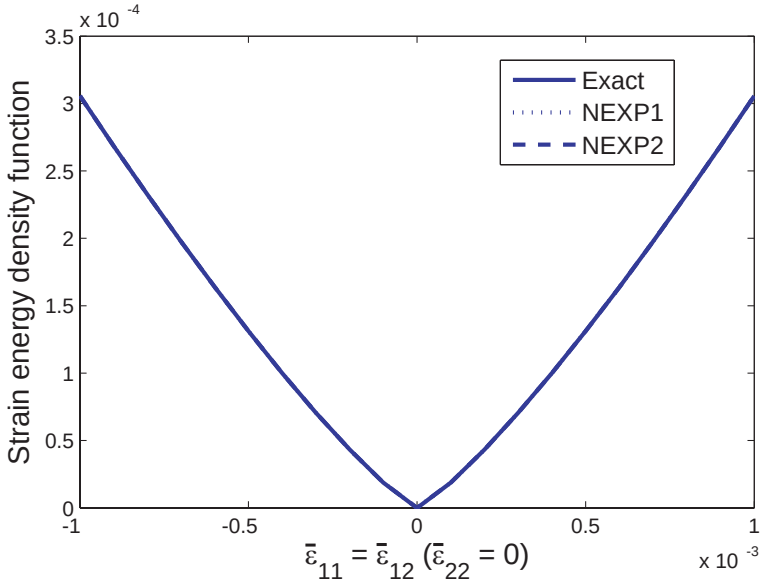

Fig. 3. NEXP1 and NEXP2 potentials for $\bar{\epsilon}_{11} = \bar{\epsilon}_{12}, \bar{\epsilon}_{22} = 0$, $p = 21$. The NEXP2 solution is constructed using $\delta = 10^{-6}$.

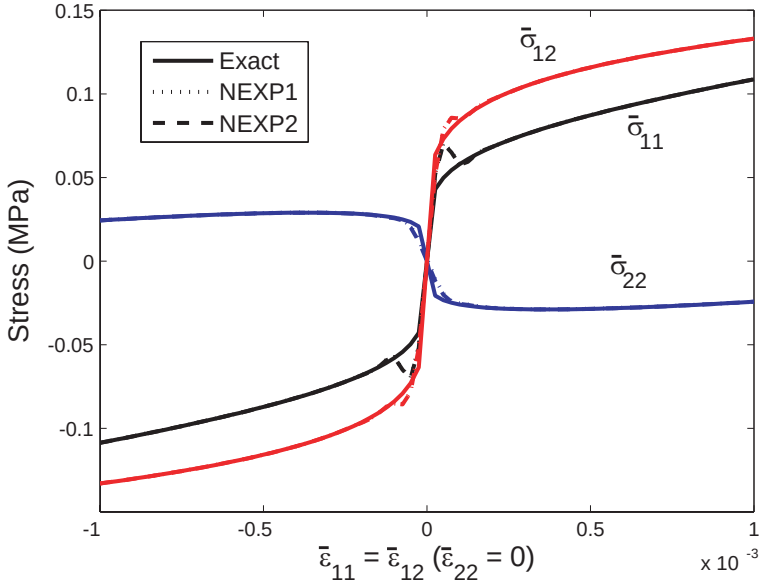

Fig. 4. NEXP1 and NEXP2 stress tensor components for $\bar{\epsilon}_{11} = \bar{\epsilon}_{12}, \bar{\epsilon}_{22} = 0$, $p = 21$. The NEXP2 solution is constructed using $\delta = 10^{-6}$.

The present test is a severe one, due to the presence of sharp variations at the origin. We show in the next tests that the oscillations can be reduced by increasing the number of sampling points p.

In figures 6 and 7, we examine the convergence of NEXP1 and NEXP2 with respect to the number of sampling points p along each direction. The value $\delta = 10^{-6}$ is used for the NEXP2 solution. Results show that the oscillations reduce when increasing p. Comparable accuracy is noticed for the two methods.

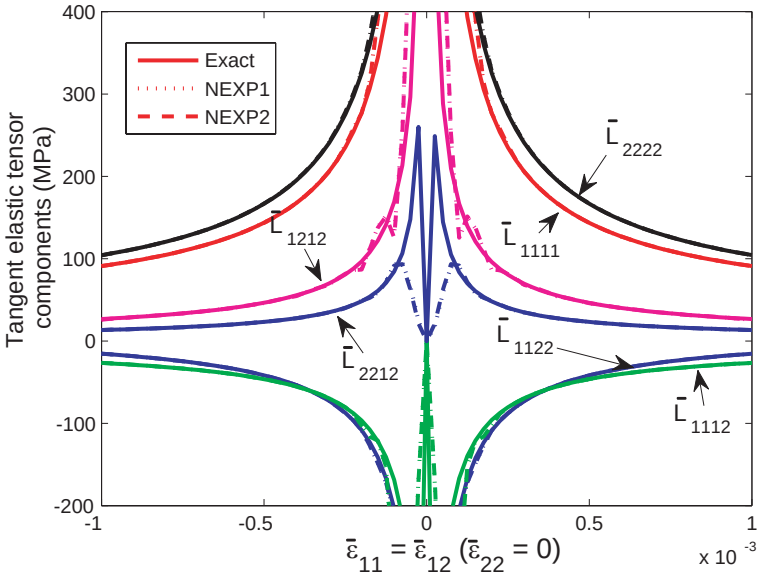

Fig. 5. NEXP1 and NEXP2 tangent elastic tensor components for $\bar{\epsilon}_{11} = \bar{\epsilon}_{12}, \bar{\epsilon}_{22} = 0$, $p = 21$. The NEXP2 solution is constructed using $\delta = 10^{-6}$.

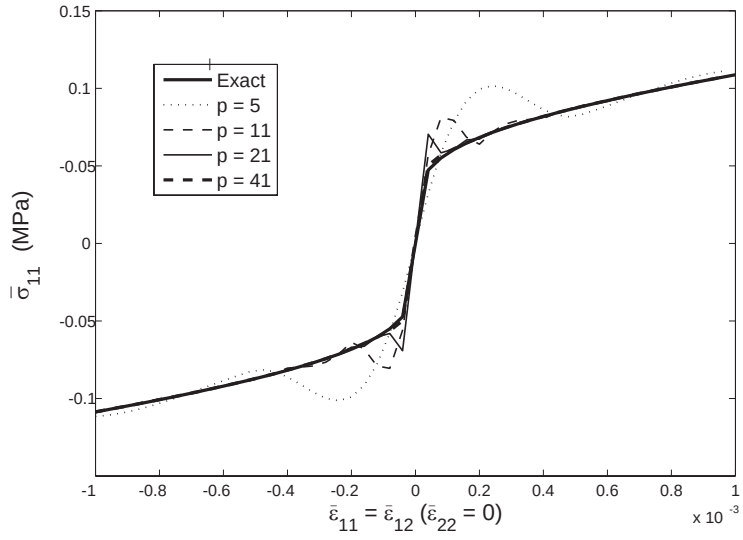

Fig. 6. Convergence of the NEXP1 stress value $\bar{\sigma}_{11}$ with respect to p.

In the last test, we examine the convergence of the NEXP2 solution with respect to δ, for a fixed value $p = 21$. The result is shown in figure 8 where the corresponding values of products R are indicated.

NEXP1 and NEXP2 are found to provide comparable accuracy if a sufficiently small value δ is chosen in NEXP2.

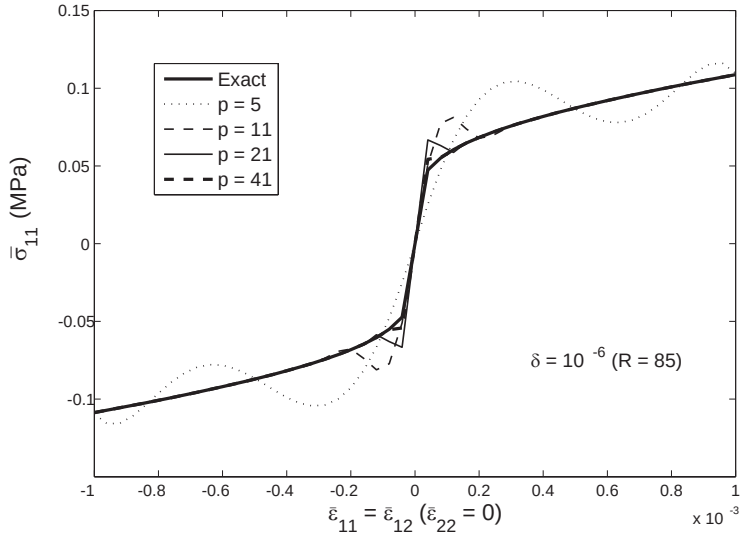

Fig. 7. Convergence of the NEXP2 stress value $\bar{\sigma}_{11}$ with respect to p, $\delta = 10^{-6}$.

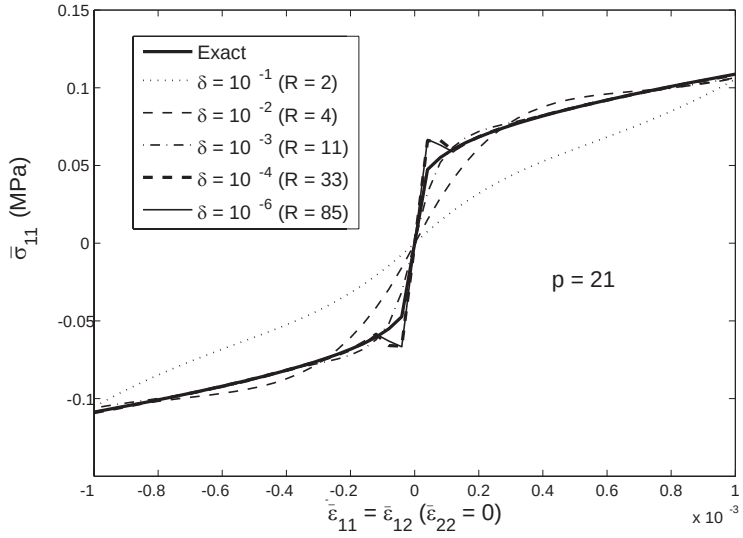

Fig. 8. Convergence of the NEXP2 stress value $\bar{\sigma}_{11}$ with respect to δ, $p = 21$.

4.2 Compressible composite with cylindrical pores

In the following different examples, we focus on two-phases composites consisting of infinitely long aligned fibers perfectly bonded to a matrix (even though the method is not restricted to this case).

As a first example, a two-phases composite made of a matrix perforated with periodic cylindrical pores is considered. The matrix is assumed to be an isotropic material characterized by the same strain-energy as (39). Thus,

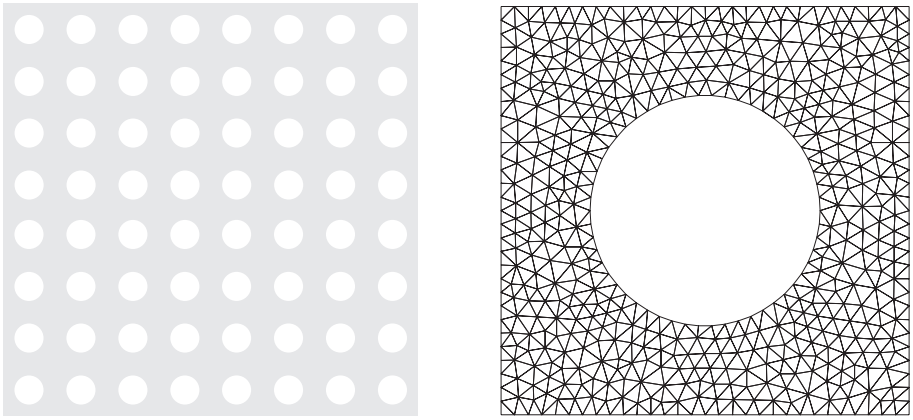

Fig. 9. Periodic porous material, microstructure and Finite Element mesh of the r.v.e. for $c = 0.25$.

the stress-strain relation for the matrix is given by:

$$\boldsymbol{\sigma} = \frac{\partial w^{(r)}(\boldsymbol{\varepsilon})}{\partial \boldsymbol{\varepsilon}} = \kappa^{(r)} Tr(\boldsymbol{\varepsilon})\mathbf{1} + \frac{2}{3}\frac{\sigma_0^{(r)}}{\varepsilon_0^{(r)}}\left(\frac{\varepsilon_{eq}}{\varepsilon_0^{(r)}}\right)^{m^{(r)}-1} \boldsymbol{\varepsilon}_d \ . \tag{40}$$

The incompressible case is met for $\kappa \to \infty$ and will be studied in section 4.4.

The microstructure and representative volume element model used for the numerical calculations are depicted in figure 9. The porosity of the composite is $c = 0.25$. The parameters of the matrix material are: $\kappa = 20$ MPa, $m = 0.4$, $\varepsilon_0 = 1$ and $\sigma_0 = 1$ MPa. The aim of this example is to test the accuracy of the NEXP2 approximation with respect to the full-field finite element solution taken as the reference one. In-plane loading is adopted. As the composite is compressible, the macroscopic strains involves three independent components : $\bar{\varepsilon}_{11}$, $\bar{\varepsilon}_{22}$ and $\bar{\varepsilon}_{12}$. The strain domain Δ of $\mathcal{E}$ used to construct a three-dimensional grid is $\Delta = [\bar{\varepsilon}_1^{\min}, \bar{\varepsilon}_1^{\max}] \times [\bar{\varepsilon}_2^{\min}, \bar{\varepsilon}_2^{\max}] \times [\bar{\varepsilon}_6^{\min}, \bar{\varepsilon}_6^{\max}] = [-10^{-3}, 10^{-3}] \times [-10^{-3}, 10^{-3}] \times [-10^{-3}, 10^{-3}]$. We set $p = 10$, so that $p^3 = 1000$ FE computations on the r.v.e. are necessary. With the NEXP2 technique, we prescribe the tolerance parameter $\delta = 10^{-6}$ implying $R = 43$.

In figure 10, we compute the overall potential $\bar{w}^*$ and macroscopic equivalent stress $\bar{\sigma}^*_{eq}$ for the uniaxial stretching defined by $\bar{\varepsilon}_{11} \neq 0$, $\bar{\varepsilon}_{22} = 0$ and $\bar{\varepsilon}_{12} = 0$. For in-plane loading the equivalent strain and stress reduce to $\varepsilon_{eq} = (2/\sqrt{3})\sqrt{\varepsilon_{12}^2 + \frac{1}{4}(\varepsilon_{11} - \varepsilon_{22})^2}$ and $\sigma_{eq} = \sqrt{3[\sigma_{12}^2 + \frac{1}{4}(\sigma_{11} - \sigma_{22})^2]}$, respectively.

The NEXP2 solution is found to be in excellent agreement with the full-field FE solution. The values of $\bar{w}^*$ and $\bar{\sigma}^*_{eq}$ are normalized with respect to w_0 and σ_{eq0}, which correspond to the highest values of w and σ_{eq} for the matrix.

To test the accuracy of our approach in a complex strain state, we prescribe the following macroscopic strain: $\bar{\boldsymbol{\varepsilon}} = \bar{\varepsilon}_1(\mathbf{e}_1 \otimes \mathbf{e}_1 + \mathbf{e}_2 \otimes \mathbf{e}_2) + \bar{\varepsilon}_1 \left(\mathbf{e}_1 \otimes \mathbf{e}_2 + \mathbf{e}_2 \otimes \mathbf{e}_1\right)/\sqrt{2}$

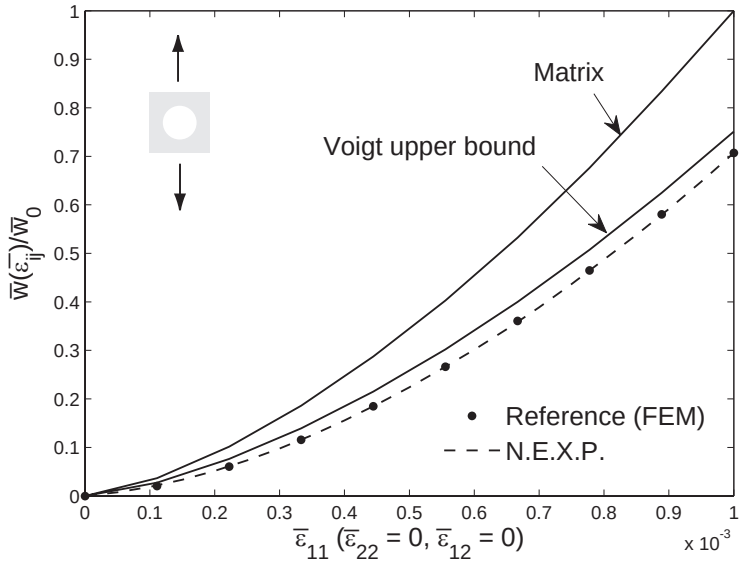

(a)

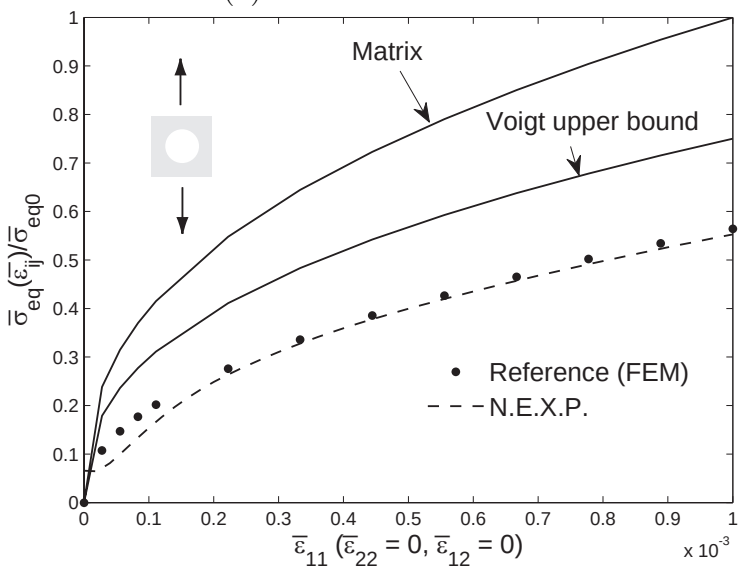

(b)

Fig. 10. Overall potential for the compressible composite with cylindrical pores for uniaxial traction.

which combines biaxial stretching with simple shear. The obtained numerical results are presented in figure 11. Here again, very good agreement between the NEXP2 and full-field solutions is noticed.

4.3 Compressible unidirectional short-fiber reinforced composite

In this example we study the anisotropic short-fiber reinforced composite whose microstructure is periodic as depicted in figure 12. The fibers, called

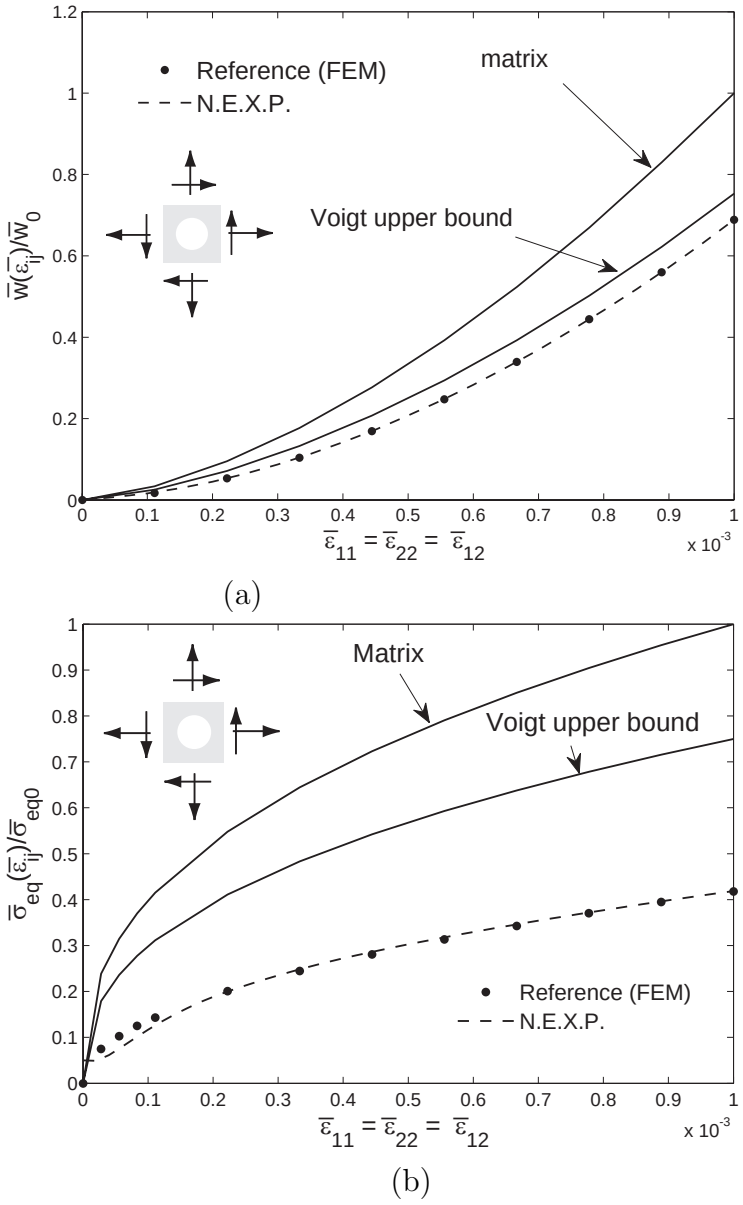

Fig. 11. a) Overall potential for the compressible composite with cylindrical pores for complex loading state; b) Overall equivalent stress for complex loading state.

phase 2, and the matrix, referred to as phase 1, are assumed to be isotropic and compressible materials characterized by (39). The material parameters are chosen in such a way that the matrix is highly nonlinear while the fibers are linear elastic and much more rigid than the matrix. This example aims to investigate the accuracy of the NEXP2 method for strongly anisotropic compressible materials. The values of the material parameters adopted are: $\kappa^{(1)} = \kappa^{(2)} = 20$ MPa, $\sigma_0^{(2)}/\sigma_0^{(1)} = 1000$, $m^{(2)} = 1$, $m^{(1)} = 0.4$. The hypermatrix $\bar{\mathbb{W}}$ is constructed as in the previous example. The NEXP2 method is used. It turns out that $R = 40$ products in Eq. (26) are necessary to reproduce $\bar{w}$ with an accuracy $\delta = 10^{-6}$.

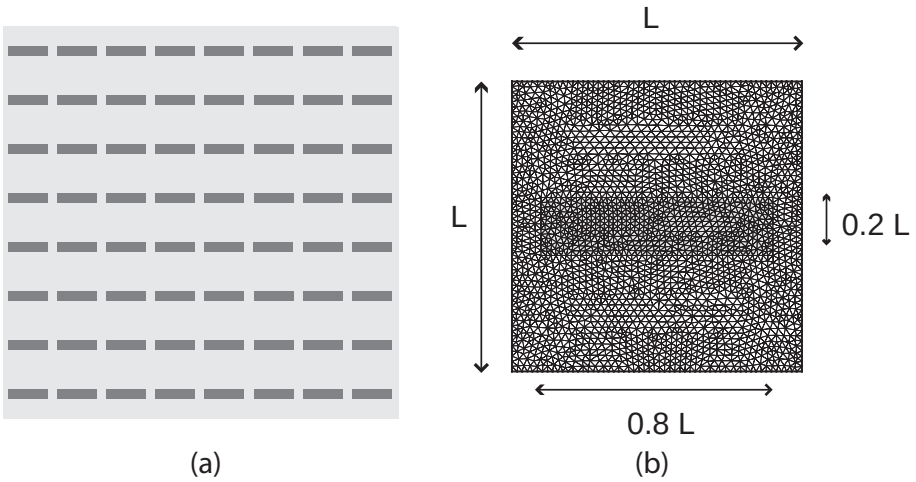

Fig. 12. (a) Anisotropic material; (b) Representative Volume Element geometry (FE mesh).

In the first test, we prescribe a biaxial stretching. Plots for the effective potential and equivalent stress are provided in figures 13 (a) and 13 (b). As expected, the stress response $\bar{\sigma}_{11}$ and $\bar{\sigma}_{22}$ are different (see figure 13 (b)), due to the anisotropy of the r.v.e. in figure 12. The NEXP2 solution is also in excellent accuracy with the full field FE solution. In this case the potential and stresses are normalized with respect to the maximum value of the fibers' response.

In the second test, we impose a uniaxial stretching combined with simple shear. A comparison between the NEXP2 and FE solutions is given in figures 14. Once again, excellent agreement with the FE solution is noticed. The equivalent stress fields in the r.v.e. calculated by FEM in the cases of biaxial stretching and uniaxial stretching combined with simple shear are shown in figures 15 (a) and 15 (b), respectively.

4.4 2D isotropic incompressible composite

To assess the accuracy of the numerical approach elaborated in this work, we compare the results provided by it with various estimates and bounds from the literature of nonlinear homogenization. We consider a two-phase composite consisting of inclusions embedded in a matrix. The composite is assumed to be statistically isotropic at the macroscopic level. The phases of the composite are taken to be isotropic and incompressible. More precisely, they are characterized by the strain-energy

$$w^{(r)}(\boldsymbol{\varepsilon}) = \frac{\varepsilon_0 \sigma_0^{(r)}}{1+m}\left(\frac{\varepsilon_{eq}}{\varepsilon_0}\right)^{1+m} \text{ if } Tr(\boldsymbol{\varepsilon}) = 0, \quad w^{(r)}(\boldsymbol{\varepsilon}) = +\infty \text{ otherwise.} \tag{41}$$

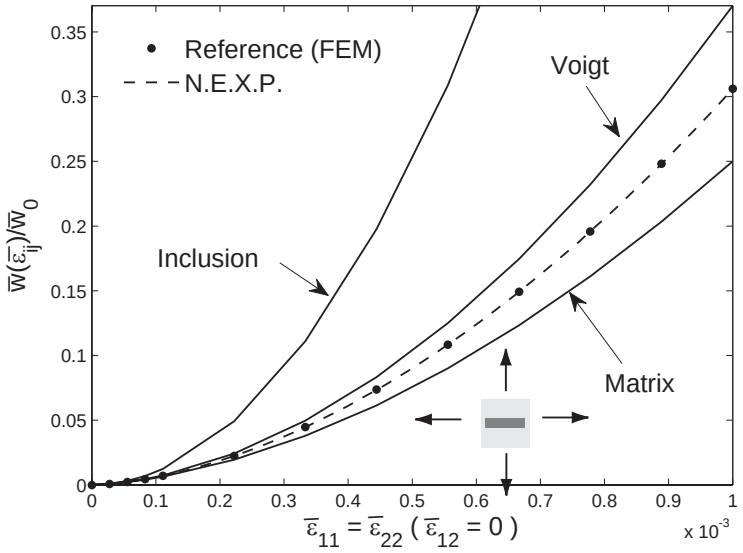

(a)

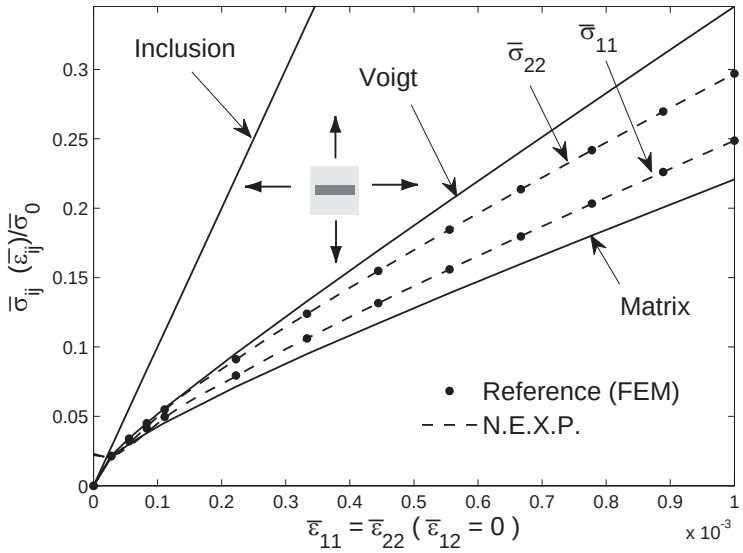

(b)

Fig. 13. (a) Overall potential and equivalent stress for the anisotropic compressible composite in biaxial traction.

Note that the two phases are different only in that $\sigma_0^{(1)} \neq \sigma_0^{(2)}$. The stress-strain relationship is then given for each phase by

$$\boldsymbol{\sigma}^{(r)} = -\mathcal{P}\mathbf{1} + \frac{2}{3}\frac{\sigma_0^{(r)}}{\varepsilon_0}\left(\frac{\varepsilon_{eq}}{\varepsilon_0}\right)^{m-1}\boldsymbol{\varepsilon}_d \ , \tag{42}$$

where $\mathcal{P}$ is the undetermined hydrostatic stress due to the incompressibility condition $Tr(\boldsymbol{\epsilon}) = 0$. The distribution of the inclusions is assumed isotropic. Since the composite is made with nonlinear materials characterized by a power-law model with the same exponent m and the same reference strain

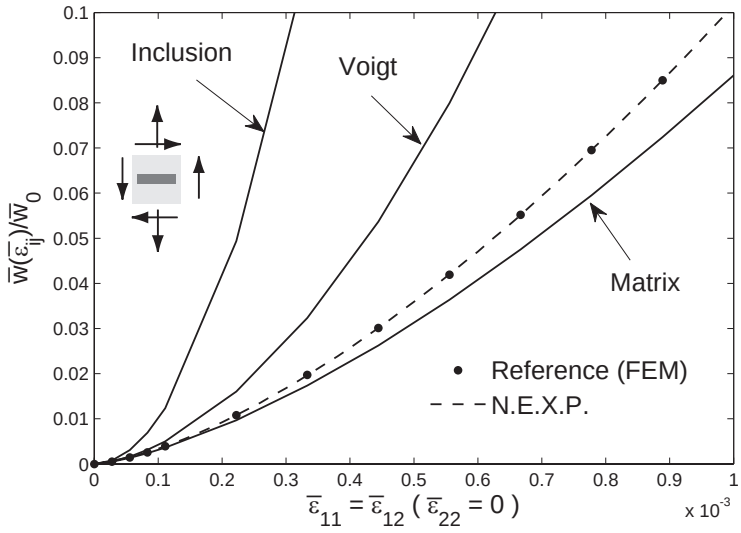

(a)

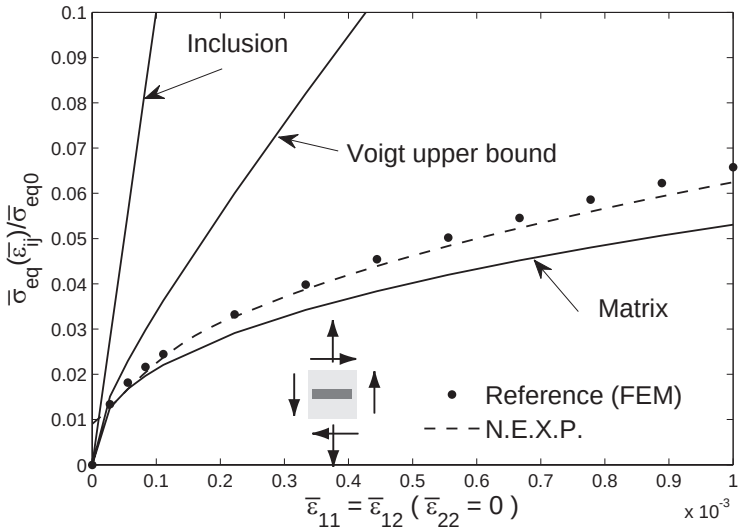

(b)

Fig. 14. (a) Overall potential and equivalent stress for the anisotropic compressible composite in uniaxial stretching with shear.

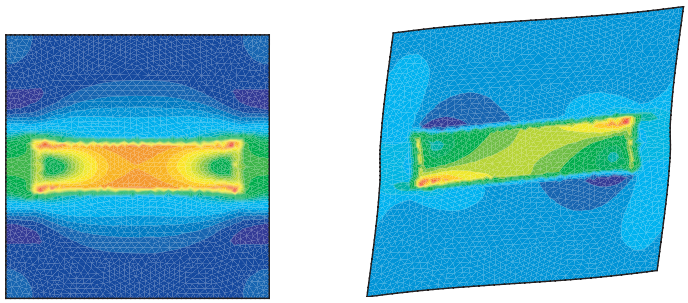

(a) (b)

Fig. 15. a) Biaxial stretching of the anisotropic microstructure; b) uniaxial stretching with shear.

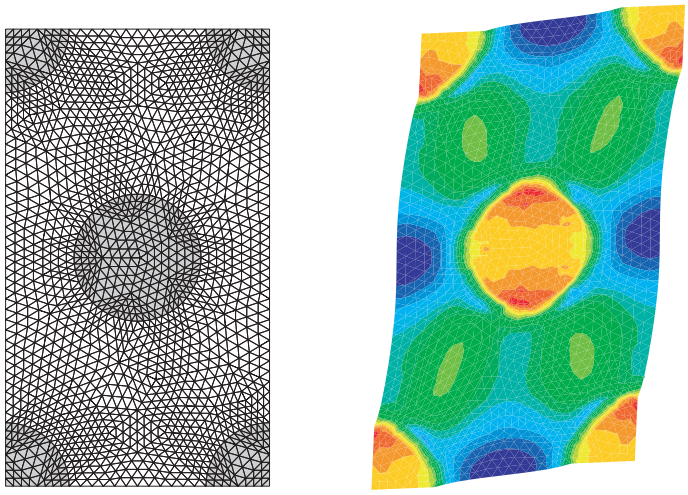

Fig. 16. a) R.v.e. corresponding to a hexagonal cell, $c = 0.21$; b) Von Mises stress field for pure shear deformation, $m = 0.4$.

ε_0, its effective potential takes the form

$$\bar{w}^{(r)}(\boldsymbol{\varepsilon}) = \frac{\varepsilon_0 \tilde{\sigma}_0}{1+m} \left(\frac{\bar{\varepsilon}_{eq}}{\varepsilon_0} \right)^{1+m} \quad . \tag{43}$$

Above, the effective flow stress $\tilde{\sigma}_0$ depends on the nonlinearity parameter m, the contrast between $\sigma_0^{(1)}$ and $\sigma_0^{(2)}$, and the fiber volume fraction. The complete characterization of the effective behavior of the composite under consideration amounts to determining $\tilde{\sigma}_0$.

We prescribe an isochoric macroscopic strain in the form:

$$\bar{\boldsymbol{\varepsilon}} = \bar{\varepsilon}_1 \left(\mathbf{e}_1 \otimes \mathbf{e}_1 - \mathbf{e}_2 \otimes \mathbf{e}_2 \right) + \frac{\bar{\varepsilon}_6}{\sqrt{2}} \left(\mathbf{e}_1 \otimes \mathbf{e}_2 + \mathbf{e}_2 \otimes \mathbf{e}_1 \right) \quad . \tag{44}$$

Thus the homogenized potential $\bar{w}$ depends only on the two components $\bar{\varepsilon}_1$ and $\bar{\varepsilon}_6$. In the case of incompressible materials, the NEXP stress is given by:

$$\bar{\sigma}_\alpha = -\mathcal{P}\mathbf{1} + \frac{\partial \bar{w}^*}{\partial \bar{\varepsilon}_\alpha} \quad . \tag{45}$$

In the present example, we choose $p = 10$ points regularly spaced along each direction of the strain domain $\Delta = [0, 10^{-3}] \times [0, 10^{-3}]$. This implies $p^2 = 100$ FE computations for the r.v.e described in figure 16. In this example, the NEXP1 technique is used.

In relation to the composite under investigation, there are exact results (LAM) for nonlinear laminates characterized by power-law models of deBotton and Hariton [44] and the variational (VAR) and second-order (SO) estimates of Idiart and Ponte Castañeda [45]. For the SO estimates, the notation SO(W) and SO(U) correspond to the stress and strain formulations, respectively. In

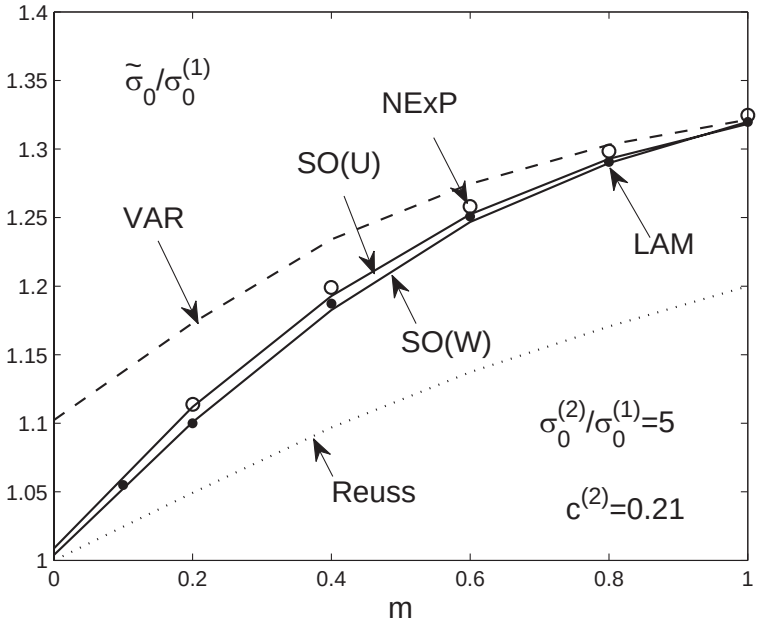

Fig. 17. Effective flow stress $\tilde{\sigma}_0$, normalized by the flow stress of the matrix $\sigma_0^{(1)}$, for power-law, fiber-reinforced ($\sigma_0^{(2)}/\sigma_0^{(1)} = 5$) as a function of the strain-rate sensitivity m. Comparisons between the 'second-order' (SO), 'variational' (VAR) estimates of the Hashin-Shtrikman type, exact results for power-law laminates (LAM) and Numerically Explicit Potential (NEXP) solutions.

addition, the classical bounds of Voigt and Reuss for the effective behaviour are also included for comparison.

In figure 17, plots are provided for the effective flow stress $\tilde{\sigma}_0$ of a fiber-reinforced composite, normalized by the flow stress of the matrix $\sigma_0^{(1)}$. The effective flow stress can be expressed as $\tilde{\sigma}_0 = \bar{\sigma}_{eq}\,(\varepsilon_0/\bar{\varepsilon}_{eq})^m$. Figure 17 shows $\tilde{\sigma}_0/\sigma_0^{(1)}$ in terms of the strain-rate sensitivity m. We observe that the NEXP solution is in very good agreement with the exact LAM results and SO estimates.

In figures 18(a)-(b), results are given for the corresponding first moments (phase averages) of the local fields. Figure 18 (a) shows the phase equivalent strain $\bar{\varepsilon}_{eq}^{(r)}$ normalized by the equivalent macroscopic strain $\bar{\varepsilon}_{eq}$. It is found that the NEXP solution is in very good agreement with the LAM exact results, and with the different estimates. In figure 18(b), the corresponding results for the phase equivalent stress $\bar{\sigma}_{eq}^{(r)}$ normalized by the equivalent macroscopic stress $\bar{\sigma}_{eq}$ is expressed as a function of m. Once again, the NEXP solution is in very good agreement with the LAM exact solution.

In figure 19, plots are provided for the effective flow stress $\tilde{\sigma}_0$ of the fiber-weakened composite normalized by the flow stress of the matrix $\sigma_0^{(1)}$ and varying with the strain-rate sensitivity m. Once again, we observe that the NEXP solution is in very good agreement with the exact LAM results and

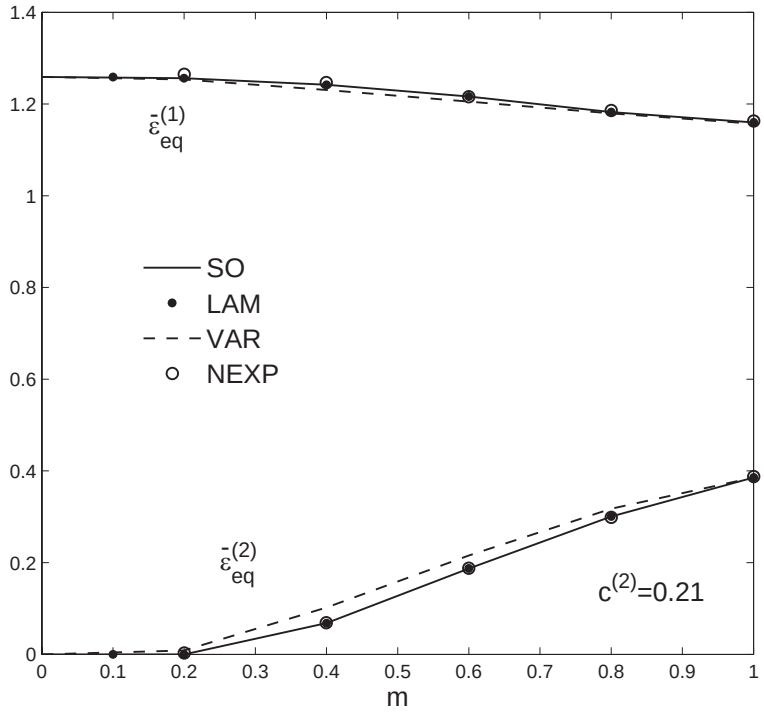

(a)

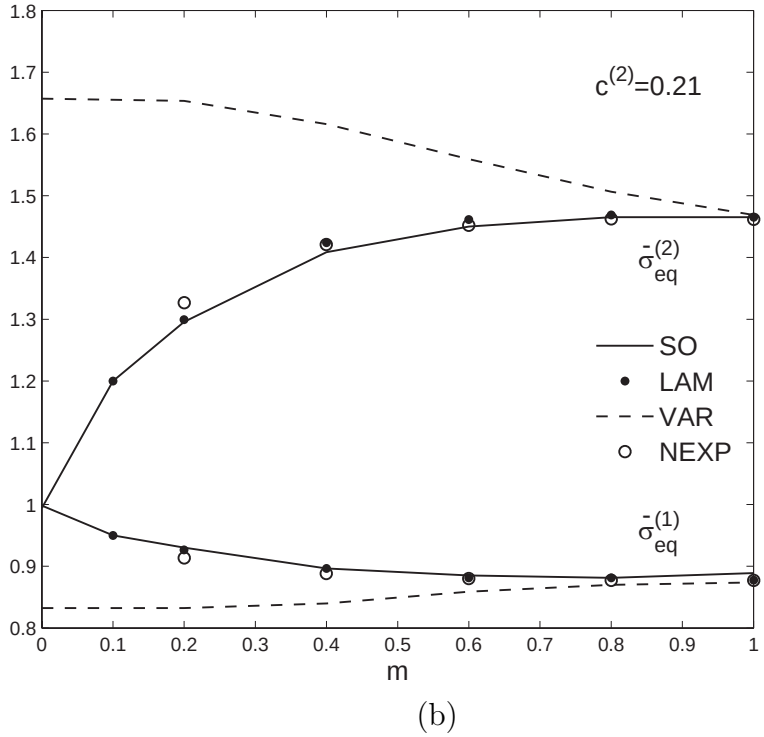

(b)

Fig. 18. Phase average of the local fields in fiber-reinforced composites. Equivalent average strain $\bar{\varepsilon}^{(r)}_{eq}$ and stress $\bar{\sigma}^{(r)}_{eq}$ in each phase, normalized by the macroscopic equivalent strain $\bar{\varepsilon}_{eq}$ and stress $\bar{\sigma}_{eq}$, respectively.

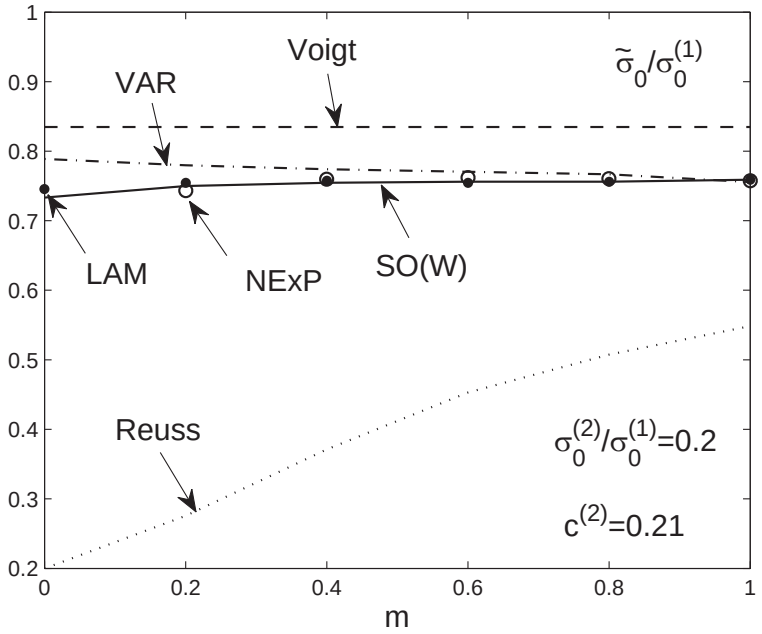

Fig. 19. Effective flow stress $\tilde{\sigma}_0$, normalized by the flow stress of the matrix $\sigma_0^{(1)}$, for power-law, fiber-weakened ($\sigma_0^{(2)}/\sigma_0^{(1)} = 0.2$) as a function of the strain-rate sensitivity m. Comparisons between the 'second-order' (SO), 'variational' (VAR) estimates of the Hashin-Shtrikman type, exact results for power-law laminates (LAM) and Numerically Explicit Potential (NEXP) solutions.

SO estimates. Due to numerical convergence problems, it was not possible to treat the non-smooth case $m = 0$ by NEXP.

In figures 20(a)-(b), results are given for the corresponding first moments (phase averages) of the local fields. Figure 20(a) shows the equivalent average strain in each phase $\bar{\varepsilon}_{eq}^{(r)}$, normalized by the equivalent macroscopic strain $\bar{\varepsilon}_{eq}$. It is found that in this case, the NEXP solution deviates from the exact solution for high nonlinearity. As the NEXP solution is directly related to the FE solution, we assume that this mismatch comes from the choice of the r.v.e. which does not fully represent an isotropic material in the case of strong nonlinearity. On the other hand, in figure 20(b), the corresponding equivalent average stress in each phases $\bar{\sigma}_{eq}^{(r)}$ is presented and found to be in very good agreement with the LAM exact solution and SO estimates.

4.5 Bending of a beam made of a nonlinear heterogeneous material

In this example, we test the efficiency of the method proposed in the present work in solving the problem of a structure made of a nonlinearly elastic heterogeneous material. The structure under consideration is a beam consisting of a short-fiber reinforced composite (Fig. 21(a)). The microstructure of the composite is the same as described in figure 12. The phase properties are

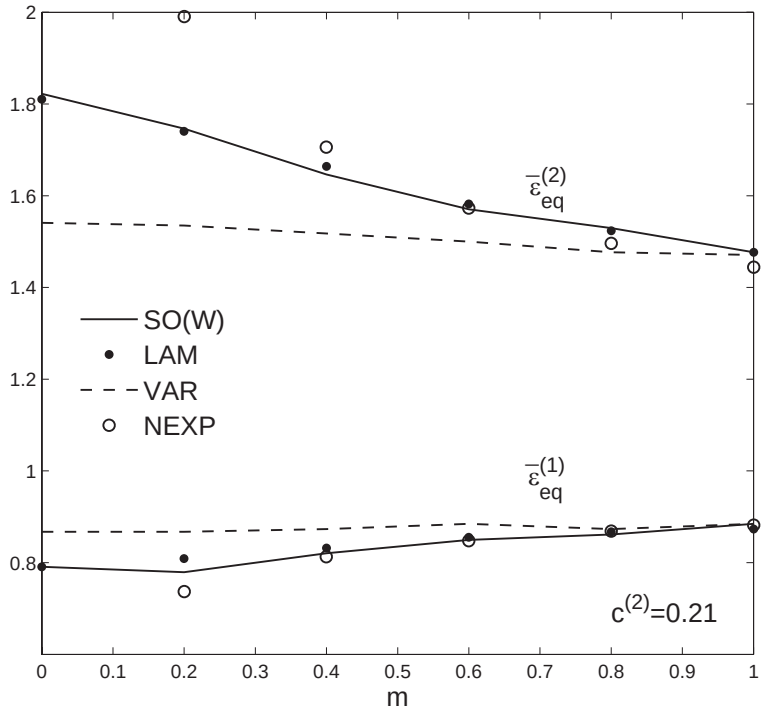

(a)

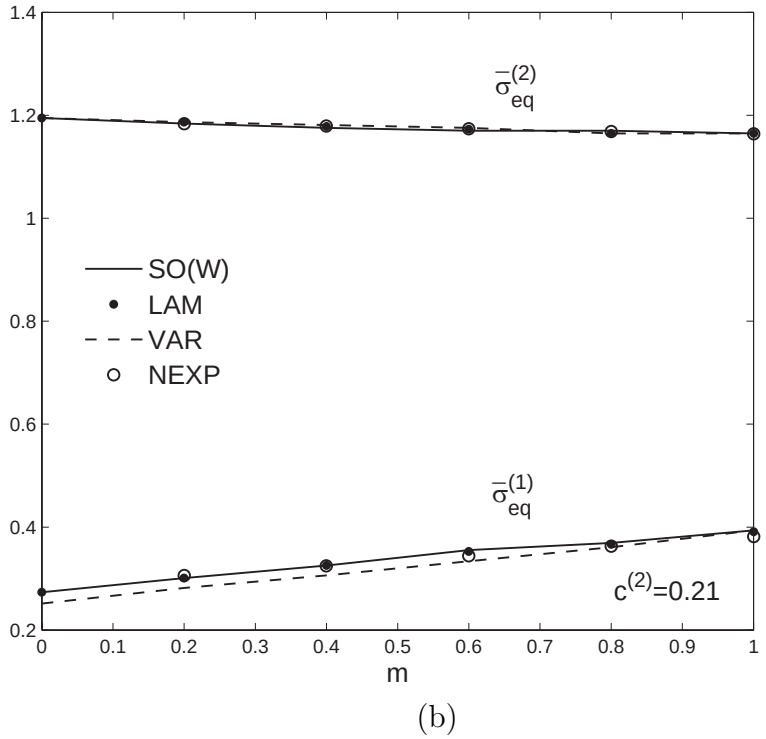

(b)

Fig. 20. Phase average of the local fields in fiber-weakened composites. Equivalent average strain $\bar{\varepsilon}^{(r)}_{eq}$ and stress $\bar{\sigma}^{(r)}_{eq}$ in each phase, normalized by the macroscopic equivalent strain $\bar{\varepsilon}_{eq}$ and stress $\bar{\sigma}_{eq}$, respectively.

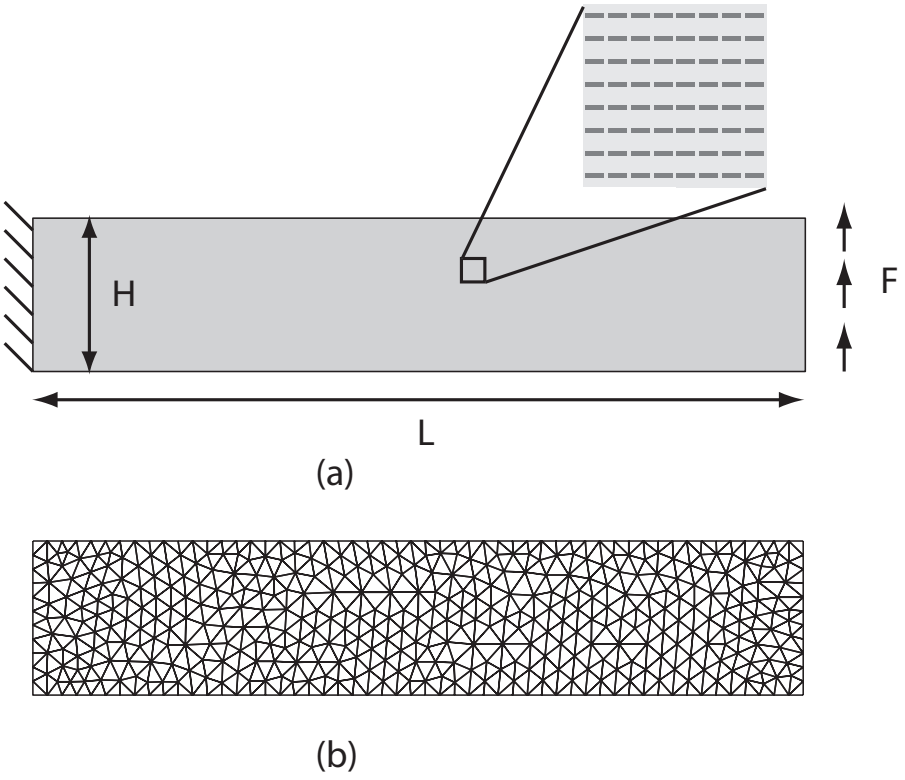

Fig. 21. (a) Geometry of the heterogeneous structure and applied boundary conditions; (b) FE mesh.

identical to those of example 4.3. Plane strain is assumed. The finite element mesh used, depicted in figure 21(b) implies 804 triangular elements with one integration point within each element. The dimensions of the beam are H = 10^{-3} m, L = 5.10^{-3} m. The applied distributed force is $F = 10^{-3}$ N.m^{-1}.

In this example, the NEXP2 approach is used. We first define the limits of the strain domain $\Delta = [\varepsilon_1^{min}, \varepsilon_1^{max}] \times [\varepsilon_2^{min}, \varepsilon_2^{max}] \times [\varepsilon_6^{min}, \varepsilon_6^{max}] = [-5.10^{-3}, 5.10^{-3}] \times [-5.10^{-3}, 5.10^{-3}] \times [-5.10^{-3}, 5.10^{-3}]$. We set $p = 11$ which gives rise to $p^3 = 1331$ preliminary computations necessary to constructing the NEXP2. Using $\delta = 10^{-6}$, we obtain $R = 73$ products of one-dimensional functions. In order to validate the solution, a simulation using concurrent multilevel (FE^2) method is achieved on the same macroscopic mesh. We use linear triangular elements with one integration point in each element. For both approaches, 4 Newton-Raphson iteration are necessary to reach structure equilibrium. According to Eq. (38), solving 12864 nonlinear problems is required to find the solution of the multiscale problem in the case of the concurrent method, as compared to 1331 for the NEXP method. To complete the analysis, we compared the relative CPU times for one macroscopic Newton-Raphson iteration for both methods. It was found that in this example, one iteration takes 206 times longer using the concurrent approach, as compared with the present method.

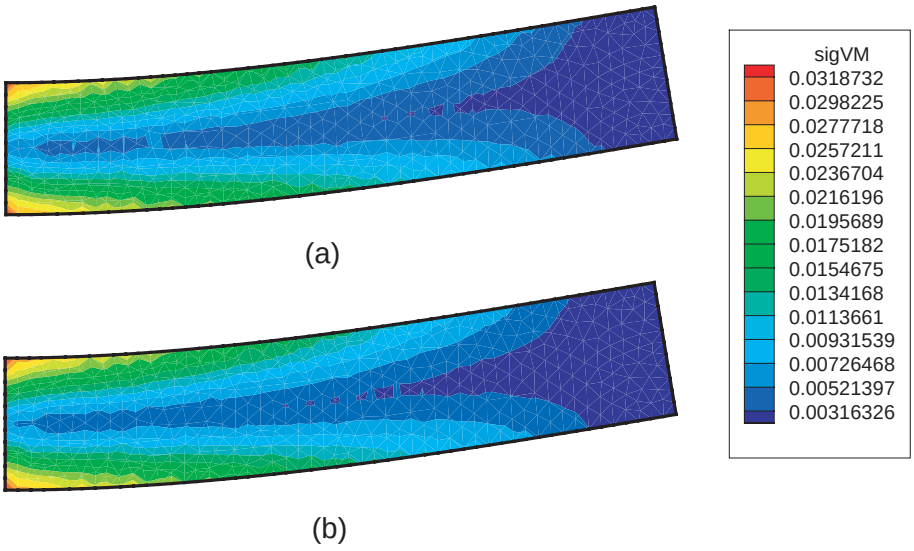

Fig. 22. Exagerated deformed configuration of the nonlinear beam and von Mises stress field: (a) NEXP ($p = 11$); (b) Concurrent multilevel method.

The results for the von Mises stress contours are depicted in figure 22, showing good agreement between the two solutions.

Next we investigate the convergence of the macroscopic solution with respect to p for the two interpolation methods, NEXP1 and NEXP2. For the case of the NEXP2 method, an additional convergence study with respect to the tolerance parameter δ is achieved. The problem described prviously is revisited by constructing $\bar{\mathbb{W}}$ for different values of p in both methods. Figure 23 shows the maximum displacement in the structure with respect to p for both methods. It is worth noting that both interpolations give equivalent accuracy when a small value δ is chosen in the NEXP2 method.

5 Conclusion

A new numerical approach has been proposed to estimate the effective behavior of nonlinearly elastic heterogeneous materials at small strains. In this approach, the effective strain-energy potential is preliminarily computed by FE for a number of points discretizing the macroscopic strain space, the resulting data are stored in the form of a hypermatrix or a set of vectors. The estimation of the effective strain-energy potential valid for the whole of the macroscopic strain space is then constructed by appropriately interpolating the preliminary discret results. The effective stress-strain relation and tangent tensor are finally derived in a numerically direct and explicit way. Two interpolation techniques have been elaoborated. The first one, named as NEXP1,

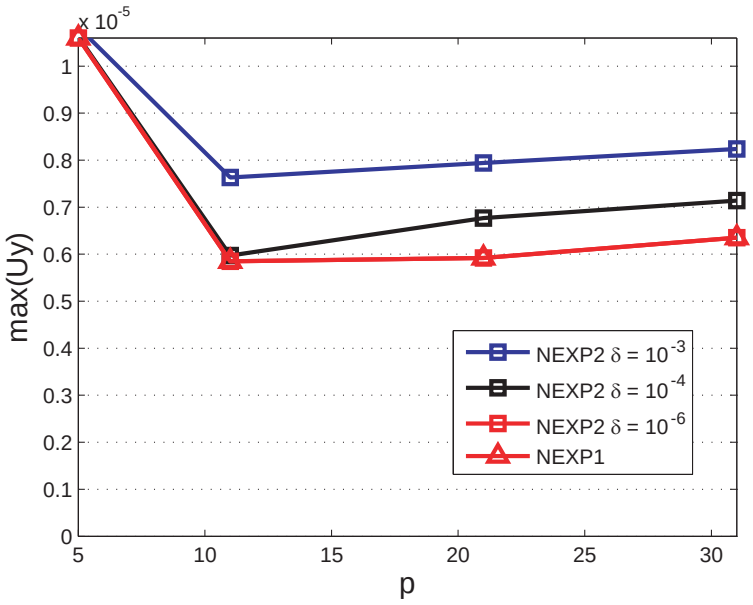

Fig. 23. Maximum y-displacement in the structure: convergence with respect to p and δ for both methods.

uses a multidimensional cubic spline interpolation. For 2D problems, the set of coefficients involved in cubic spline interpolations can be determined with no need for high computational capacity. However, for 3D problems, computing the set of coefficients requires extensive numerical efforts. The second one, called NEXP2, takes advantage of an outer product decomposition of the hypermatrix, avoiding the drawbacks of NEXP1. Both NEXP1 and NEXP2 give similar results in terms of accuracy. In the proposed approach , the most costly step is the first one where p^d finite element computations need being performed. However, these computations are independent from each other and thus well adapted to today's generation of massively parallel computers.

The proposed approach is in particular suited for the FE computations of structures made of nonlinear heterogeneous materials. Indeed, once the effective strain-energy potential is determined numerically for a given nonlinear heterogeneous material, the computation of any structure consisting of the latter is transformed into that of a structure composed of the homogenized material. As illustrated by several examples, the proposed approach is comparable with concurrent multilevel methods in terms of accuracy but much less expensive. However, the present work is limited to nonlinearly elastic heterogeneous materials at infinitesimal strains. Extension of the basic idea of the proposed approach to the homogenization of other nonlinear heterogeneous materials is being envisaged and will be presented in forthcoming works. Another future direction of this work is the introduction of uncertainties at the microscopic level to study their influence on the macroscopic response of the material.

6 Aknowledgement

Discussions with Prof. Shaofan Li, University of California, Berkeley, are greatly acknowledged.

7 Appendix 1: one dimensional cubic spline interpolation for equidistant nodes

Here we briefly review the basis of cubic spline interpolation. A fast and simple algorithm for one-dimensional cubic spline interpolation was provided in [28]. let a set of n points $\{\xi_0, \xi_1, ..., \xi_n\}$ in $\mathbb{R}$ such that $a = \xi_0 < \xi_1 < ... < \xi_n < b$ and $\xi_1 - \xi_0 = \xi_2 - \xi_1 = ... = \xi_n - \xi_{n-1} = h$. We denote by $\Delta \subset \mathbb{R}$ a one-dimensional domain. The coordinates of the points are given by $\xi_i = a + ih$. Let y_i interpolation data, $y_i \in \mathbb{R}$, $i = 0, ..., n$. For arbitrarily distributed nodes, a cubic spline is a piece-wise third-order polynomial, which can be found using recursive formula [28]. For equidistant nodes, the interpolation function $s(\xi) \in \mathcal{S}_3(\Delta)$ can be written as:

$$s(\xi) = \sum_{k=1}^{n+3} c_k u_k(\xi) \tag{46}$$

where $\mathcal{S}_3(\Delta)$ is the space of the degree three and smoothness two spline s on the grid $\Delta(a, b)$. In Eq. (46), c_k are coefficients and $u_k \in \mathcal{S}_3(\Delta)$ a basis function. On possible choice for u_k is given by

$$u_k(\xi) = \Phi\left(\frac{\xi - a}{h} + 2 - k\right) \quad , k = 1, ..., n+3 \tag{47}$$

with $\Phi(t)$ is given by Eq. (22). In figure 24, the set of basis functions $\mathbf{U} = \{u_1, u_2, ..., u_{n+3}\}$ is depicted.

We need $n+3$ interpolation conditions in order to determine the interpolating spline function uniquely. However $s(\xi_i) = y_i$, $i = 0, ..., n$ only specifies $n + 1$ conditions. Therefore, it is necessary to add two conditions which can be applied to either first-order or second-order derivatives. In the context of the present work, as we solve full FE problem at each point of the strain space, the derivatives (stresses) are readily available. One possible choice is to prescribe the values of the values of the first-order derivatives in two points of the 1-D stain space. This solution can be extended to higher dimensional spaces.

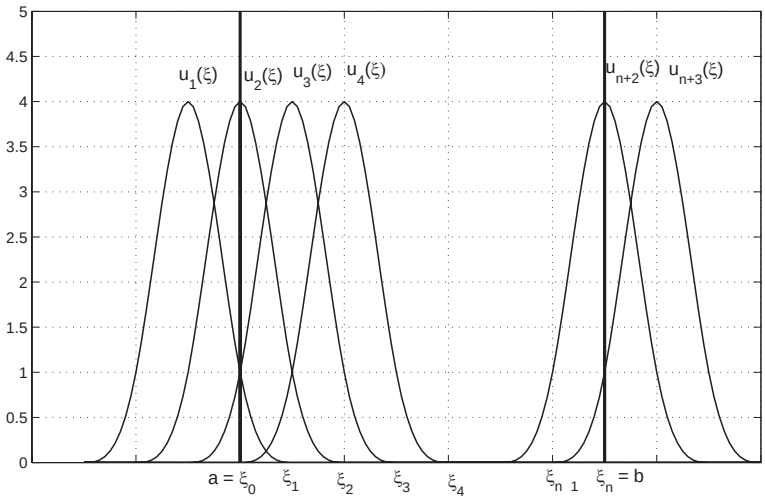

Fig. 24. Base of $\mathcal{S}_3(\Delta)$. Basis functions $u_1, u_2, ..., u_{n+3}$ of the function space of splines $\mathcal{S}_3(\Delta)$ on the interval $[a, b]$ with equidistant points.

Then writing the $n+3$ conditions defines the linear system of equations:

$$s(\xi_i) = \sum_{k=l}^{m} c_k u_k(\xi_i) = y_i, \quad l = \left\lfloor \frac{\xi_i - a}{h} \right\rfloor + 1, \quad i = 0, ..., n \tag{48}$$

$$s'(\xi_\alpha) = \sum_{k=l}^{m} c_k u'_k(\xi_\alpha) = y'_\alpha, \quad l = \left\lfloor \frac{\xi_\alpha - a}{h} \right\rfloor + 1, \tag{49}$$

$$s'(\xi_\beta) = \sum_{k=l}^{m} c_k u'_k(\xi_\beta) = y'_\beta, \quad l = \left\lfloor \frac{\xi_\beta - a}{h} \right\rfloor + 1, \tag{50}$$

with $m = min(l+3, n+3)$ and where $\lfloor . \rfloor$ denotes the floor function. The linear system of equations can be rewritten as:

$$\mathbf{Ac} = \mathbf{y} \tag{51}$$

where the matrix $\mathbf{A}$ is symmetric and tridiagonal and $\mathbf{c}$ is the vector of unkown coefficients. Extension to multidimensional spline interpolation is provided in [28].

8 Appendix 2: expression of the elastic tangent tensor components

Here we give the correspondance between the components of $\hat{\mathbb{L}}$ defined in Eq. (15) and the components of the effective elastic tangent tensor $\bar{\mathbb{L}}$.

$$\begin{bmatrix} \bar{L}_{1111} & \bar{L}_{1122} & \bar{L}_{1133} & \bar{L}_{1112} & \bar{L}_{1113} & \bar{L}_{1123} \\ & \bar{L}_{2222} & \bar{L}_{2233} & \bar{L}_{2212} & \bar{L}_{2213} & \bar{L}_{2223} \\ & & \bar{L}_{3333} & \bar{L}_{3312} & \bar{L}_{3313} & \bar{L}_{3323} \\ & & & \bar{L}_{1212} & \bar{L}_{1213} & \bar{L}_{1223} \\ & & & & \bar{L}_{1313} & \bar{L}_{1323} \\ & & & & & \bar{L}_{2323} \end{bmatrix} = \begin{bmatrix} \hat{L}_{11} & \hat{L}_{12} & \hat{L}_{13} & \frac{\hat{L}_{16}}{\sqrt{2}} & \frac{\hat{L}_{15}}{\sqrt{2}} & \frac{\hat{L}_{14}}{\sqrt{2}} \\ & \hat{L}_{22} & \hat{L}_{23} & \frac{\hat{L}_{26}}{\sqrt{2}} & \frac{\hat{L}_{25}}{\sqrt{2}} & \frac{\hat{L}_{24}}{\sqrt{2}} \\ & & \hat{L}_{33} & \frac{\hat{L}_{36}}{\sqrt{2}} & \frac{\hat{L}_{35}}{\sqrt{2}} & \frac{\hat{L}_{34}}{\sqrt{2}} \\ & & & \frac{\hat{L}_{66}}{2} & \frac{\hat{L}_{65}}{2} & \frac{\hat{L}_{64}}{2} \\ & & & & \frac{\hat{L}_{55}}{2} & \frac{\hat{L}_{54}}{2} \\ & & & & & \frac{\hat{L}_{44}}{2} \end{bmatrix} \quad (52)$$

References

[1] Hill, R., 1965. Continuum micromechanics of elastoplastic polycrystals. J. Mech. Phys. Solids 13, 89–101.

[2] Willis, J.R., 1983. The overall response of composite materials. ASME J. Appl. Mech. 50, 1202–1209.

[3] Dvorak, G.J., 1992. Transformation field analysis of inelastic composite materials. Proc. R. Soc. Lond. A 437, 311–327.

[4] Qiu, Y.P., Weng, G. J., 1992. A theory of plasticity for porous materials and particle-reinforced composites. Int. J. Plasticity 59, 261–268.

[5] Ponte Castañeda, P., 1991. The effective mechanical properties of nonlinear isotropic composites. J. Mech. Phys. Solids 39, 45–71.

[6] Hu, G.K., 1996. A method of plasticity for general aligned spheroidal void or fiber-reinforced composites. Int. J. Plasticity 12, 439–449.

[7] Milton, G.W., Serkov, S.K., 2000. Bounding the current in nonlinear conducting composites. J. Mech. Phys. Solids 48, 1295–1324.

[8] Nemat-Nasser, S., 1993. Micromechanics: Overall Properties of Heterogeneous Solids. Elsevier, Amsterdam.

[9] Torquato, S., 2001. Random Heterogeneous Materials: Microstructure and Macroscopic Properties. Springer.

[10] Milton, G.W, 2002. Theory of Composites. Cambridge University Press.

[11] Chu, T., Hashin, Z., 1971. Plastic behavior of composites and porous media under isotropic stress. Int. J. Engng. Sci. 9, 971–994.

[12] He, Q.-C., 1999. Uniform strains field and microstructure-independent relations in nonlinear elastic fibrous composites. J. Mech. Phys. Solids 47(8), 1781–1793.

[13] He, Q.-C., Bary, B., 2004. Exact relations for the effective properties of nonlinearly elastic inhomogeneous materials. Int. J. Multiscale Comput. Eng. 2, 69–83.

[14] He, Q.-C., Le Quang, H., Feng, Z.-Q., 2006. Exact results for the homogenization of elastic fiber-reinforced solids at finite strains. J. Elast. 83, 153–177.

[15] Le Quang, H., He, Q.-C., 2008. Effective pressure-sensitive elastoplastic behavior of particle-reinforced composites and porous media under isotropic loading. Int. J. Plasticity 24, 343–370.

[16] Smit, R., Brekelmans, W., Meijer, H., 1998. Prediction of the mechanical behavior of nonlinear heterogeneous systems by multi-level finite element modeling. Comput. Meth. Appl. Mech. Eng. 155, 181–192.

[17] Feyel, F., 1999. Multiscale FE^2 elastoviscoplastic analysis of composite structure. Comput. Mater. Sci. 16(1-4), 433–454.

[18] Feyel, F., Chaboche, J.-L., 2000. FE^2 multiscale approach for modelling the elastoviscoplastic behaviour of long fiber SiC/Ti composite materials. Comput. Meth. Appl. Mech. Eng. 183, 309–330.

[19] Feyel, F., 2003. A multilevel finite element method (FE^2) to describe the response of highly non-linear structures using generalized continua. Comput. Meth. Appl. Mech. Eng. 192, 3233–3244.

[20] Terada, K., Kikuchi, N., 2001. A class of general algorithms for multi-scale analysis of heterogeneous media. Comput. Meth. Appl. Mech. Eng. 190, 5427–5464.

[21] Ghosh, S., Lee, K., Raghavan, P., 2001. A multilevel computational model for multi-scale damage analysis in composite and porous media. Int. J. Solids Struct. 38, 2335–2385.

[22] Yvonnet, J., He, Q.-C., 2007. The Reduced Model Multiscale Method (R3M) for the non-linear homogenization of hyperelastic media at finite strains. J. Comput. Phys. 223, 341–368.

[23] Monteiro, E., Yvonnet, J., He, Q.-C., 2008. Computational Homogenization for nonlinear conduction in heterogeneous materials using model reduction. Comput. Mater. Sci. 42, 704–712.

[24] Kouznetsova, V.G., Geers, M.G.D, Brekelmans, W.A.M., 2004. Multi-scale second order computational homogenization of multi-phase materials: a nested finite element solution strategy. Comput. Meth. Appl. Mech. Eng. 193, 5525–5550.

[25] McVeigh, C., Vernerey, F., Liu, W.K., Brinson, C., 2006. Multiresolution analysis for material design. Comput. Meth. Appl. Mech. Eng. 195, 5525–5550.

[26] Ponte Castañeda, P., Willis, J.R., 1988. On the overall properties of nonlinearly viscous composites. Proc. R. Soc. Lond. A 416, 217–244.

[27] Hill, R., 1963. Elastic properties of reinforced solids: some theoretical principles. J. Mech. Phys. Solids 11, 357–372.

[28] Habermann, C., Kindermann, F., 2007. Multidimensional spline interpolation: theory and applications. Comput. Econ. 30, 153–169.

[29] Beatson, R.K., 1986. On the convergence of some cubic spline interpolation schemes. SIAM J. Numer. Anal. 23(4), 903–912.

[30] Hitchkock, F.L., 1927. The expression of a tensor or a polyadic as a sum of pructs. J. Math. Phys. 6, 164–189.

[31] Harshman, A., 1970. Foundations of the PARAFAC procedure: Models and conditions for an "explanatory" multi-modal factor analysis. UCLA working papers in phonetics, 16.

[32] Carol, J.D., Chang, J.J., 1970. Analysis of individual differences in multidimensional scaling via an N-way generalization of 'Eckart-Young' decomposition. Psychometrika 35, 283–319.

[33] Möcks, J., 1988. Topographic components model for event-related potentials and some biophysical considerations. IEEE Trans. Biomed. Eng. 35, 482–484.

[34] Kiers, H.A.L., 2000. Toward a standardized notation and terminology in multiway analysis. J. Chemometr. 14, 105–122.

[35] De Lathauwer, L., De Moor, B., Vandewalle, J., 2000. A multilinear singular value decomposition. SIAM J. Matrix Anal. Appl. 21, 1253–1278.

[36] Kapteyn, A., Neudecker, H., Wansbeek, T., 1986. An approach to n-mode components analysis. Psychometrika 51, 269–275.

[37] Tucker, L.R., 1966. Some mathematical notes on three-mode factor analysis. Psychometrika 31, 279–311.

[38] Muti, D., Bourennane, S., 2005. Multidimensional filtering based on a tensor approach. Signal Process. 85, 2338–2353.

[39] Beylkin, G., Mohlenkamp, J., 2005. Algorithms for analysis in high dimensions. SIAM J. Sci. Comput. 26, 2133–2159.

[40] Zhang, T., Golub, G.H., 2001. Rank-one approximation to high order tensor. SIAM J. Matrix Anal. Appl. 23(2), 534–550.

[41] Bader, B.W., Kolda, T.G., 2007. MATLAB Tensor Toolbox Version 2.2, http://csmr.ca.sandia.gov/ tgkolda/TensorToolbox/, January 2007.

[42] Moulinec, H., Suquet, P., 1998. A numerical method for computing the overall response of nonlinear composites with complex microstructures. Comput. Meth. Appl. Mech. Engng 157, 69–94.

[43] Moës, N., Cloirec, M., Cartraud, P., Remacle, J.-F., 2003. A computational approach to handle complex microstructure geometries. Comput. Meth. Appl. Mech. Eng. 192, 3163–3177.

[44] deBotton, G., Hariton, I., 2002. High-rank nonlinear sequentially laminated composites and their possible tendency towards isotropic behavior. J. Mech. Phys. Solids. 50, 2577–2595.

[45] Idiart, M.I., Ponte Castañeda, P., 2007. Fields in nonlinear composites. I. theory. Proc. R. Soc. Lond. A 463, 183–202.